https://doi.org/10.5194/egusphere-2026-4580
Preprint. Discussion started: 7 September 2026

"I-CYCLE v1.0": A new model of global marine iodine cycling including suboxic and benthic processes

Rosie Chance[1], Martin R. Wadley[2], Lucy J. Carpenter[1], Ryan Pound[1,4], Mat J. Evans[1], Timothy D. Jickells[3], David P. Stevens[2]

[1]Wolfson Atmospheric Chemistry Laboratories, Department of Chemistry, University of York, York, YO10 5DD, UK
[2]School of Mathematics, University of East Anglia, Norwich, NR4 7TJ, UK
[3]Centre for Ocean and Atmospheric Sciences, School of Environmental Sciences, University of East Anglia, Norwich, NR4 7TJ, UK

[4] Now at Department of Meteorology, University of Reading, Reading, RG6 6ET, UK

Correspondence to: Rosie Chance (rosie.chance@york.ac.uk)

https://doi.org/10.5194/egusphere-2026-4580
Preprint. Discussion started: 7 September 2026

Abstract. Atmospheric iodine has significant impacts on air quality, climate and human health. Its primary atmospheric source is a reaction on the sea surface between ozone and aqueous iodide (I^-), which is naturally present in the ocean alongside iodate (IO_3^-) and organic iodine species. Here we describe a new global biogeochemical model of the marine iodine cycle, I-CYCLE, which predicts the distribution and cycling of iodide, iodate, phytoplankton associated iodine, detrital iodine and benthic iodine. I-CYCLE is embedded within the UKESM 1.0 ocean framework and driven by the MEDUSA biogeochemical model. In the model, the reduction of iodate to iodide is driven by uptake to plankton and subsequent release from particulate iodine reservoirs. Iodide is returned to iodate via two processes: biological oxidation coupled to ammonia oxidation, and a slow background reaction which may be abiotic. Below a specified oxygen threshold, iodate is reduced to iodide and the release of benthic and detrital iodine as iodide is amplified. Model parameters were tuned against observed iodide and iodate fields; the best-fit parameters are in good agreement with empirical estimates. The model replicates observed present day latitudinal and vertical trends in dissolved iodine speciation, as well as the impacts of oxygen minimum zones. Future iodine fields predicted for 2100 under the SSP585 scenario are presented.

1 Introduction

The marine iodine cycle impacts key processes that affect both air quality and climate. The reaction of iodide (I^-) at the ocean surface is a major sink for tropospheric ozone (O_3), an air pollutant which harms health and ecosystems and is also a potent greenhouse gas (Carpenter et al., 2021). This reaction in turn releases reactive iodine gases to the atmosphere, which remove further ozone and contribute to both new particle formation and aerosol mass (O'Dowd et al., 2002; Baccarini et al., 2020; Gomez-Martin et al 2022). Iodine is also an essential nutrient for humans and deficiency causes congenital hypothyroidism and goitre (Zimmerman et al., 2008). Sea-to-air transport of iodine and subsequent deposition onto land is a route by which marine iodine can enter the food chain (Fuge and Johnson, 2015); these fluxes are poorly constrained but may have increased in the twentieth century (Legrand et at., 2018). Numerical predictions of marine iodine speciation, and especially sea surface iodide concentrations, are therefore required for both modelling of global and regional air quality and climate (e.g. Gantt et al., 2017; Pound et al., 2024), and for holistic assessment of dietary iodine sources. In addition, as marine iodine speciation is related to dissolved oxygen concentration and only iodate (IO_3^-) is incorporated into calcium carbonate, I/Ca ratios in the calcareous sediment record have been used for the reconstruction of paleo-ocean oxygenation (e.g. Lu et al., 2018). Quantitative application and refinement of the I/Ca tracer requires a numerical mechanistic model of the marine iodine cycle (Cheng et al., 2024).

The marine iodine cycle is dominated by interconversion of the two main iodine species, iodide and iodate, which in the modern ocean are present in the dissolved phase with a summed concentration of 450-500 nM (Wong, 1991). Iodate is reduced to iodide in the euphotic zone via a biologically mediated process (Luther et al., 2023) and slowly oxidised back again. Reduction of iodate to iodide at depth also takes place in oxygen deficient zones (ODZs; e.g. Wong and Brewer, 1977;

https://doi.org/10.5194/egusphere-2026-4580
Preprint. Discussion started: 7 September 2026

Moriyasu et al., 2020). Some iodine is taken up by phytoplankton, resulting in a small (<0.25% or < 1 nM, typically much less) particulate iodine reservoir (Wong et al., 1976; Jickells et al., 1990; Satoh et al., 2023). Iodine fluxes in and out of the ocean are small relative to the overall iodine budget: sediments have been identified as a source of iodide, especially under low oxygen conditions (Farrenkopf and Luther, 2002; Cutter et al., 2018), while volatilisation to the atmosphere is a very small sink (Carpenter et al., 2021).

To the best of our knowledge only two models of the marine iodine cycle exist (Wadley et al., 2020; Cheng et al 2024). Wadley et al. (2020) developed a three-layer model for predicting iodide and iodate concentrations in the upper ocean (to 500 m depth or the sea floor). In this model the reduction of iodate to iodide was driven by primary production and iodide oxidation was linked to nitrification. While the model gave good agreement with observations available at the time of development (Wadley et al., 2020), subsequent reports from the Pacific (Cutter et al., 2018; Moriyasu et al., 2020; Moriyasu et al., 2023) suggest it may underestimate iodide in this basin. The original Wadley et al. (2020) model did not incorporate processes taking place in low oxygen environments or sediment interactions and so is of limited use for linking iodine speciation to oxygenation, as required for paleo-oceanographic applications. Furthermore, recent observations suggest that iodide arising from sediments and ODZs can result in concentrations far in excess of the global average (> 550 nM, so called “excess iodine”) and these may persist for long enough to reach the ocean surface (Cutter et al., 2018; Chance & Tinel et al., 2020). To evaluate the regional impact of iodide arising from low oxygen environments on the air-sea exchange of iodine and ozone, a marine iodine cycling model which includes low oxygen processes and sedimentary fluxes is required.

An alternative model of marine iodine cycling embedded in the cGENIE Earth System Model was introduced by Lu et al. (2018) and substantially developed by Cheng et al. (2024). In addition to iodide and iodate reservoirs, this model also includes an organic iodine reservoir. As in Wadley et al., iodide is reduced in association with primary productivity and returned by oxidation. In addition, iodide is reduced in low oxygen conditions. This model was developed for paleoceanographic studies, for which cGENIE has the advantage of being readily able to run with ancient environmental conditions, including different continental configurations (see Cheng et al., 2024). However, it has a much lower spatial resolution than the model of Wadley et al., a more simplified representation of ocean physics, and also excludes sedimentary fluxes. It replicates large scale trends in present day iodine speciation, but over-estimates iodide concentrations at low latitudes by a factor of ~2 (Cheng et al., 2024).

Here we present a new ocean iodine cycling model, “I-CYCLE”. Although informed by our earlier work (Wadley et al., 2020), this model is a complete rebuild. In addition to iodide and iodate, new iodine reservoirs associated with plankton, detritus and sediments have been introduced. The interconversion of iodide and iodate has been re-parameterised, and key new suboxic transformations added. This improved representation of the marine iodine cycle is driven by physical ocean circulation and mixing and biogeochemistry from the UKESM 1.0 Earth System Model (Sellar et al., 2019), which enables past, present and future climate scenarios to be simulated. In this manuscript we provide a full description of the new model including key

https://doi.org/10.5194/egusphere-2026-4580
Preprint. Discussion started: 7 September 2026

80 questions addressed during its development (Sect. 2). We then present simulated global iodine fields for the present day and future scenarios (Sect. 3). We believe "I-CYCLE" is the fullest representation of the marine iodine cycle to-date, and the highest resolution and complexity model able to predict iodine speciation throughout the water column under past, present and future climate scenarios.

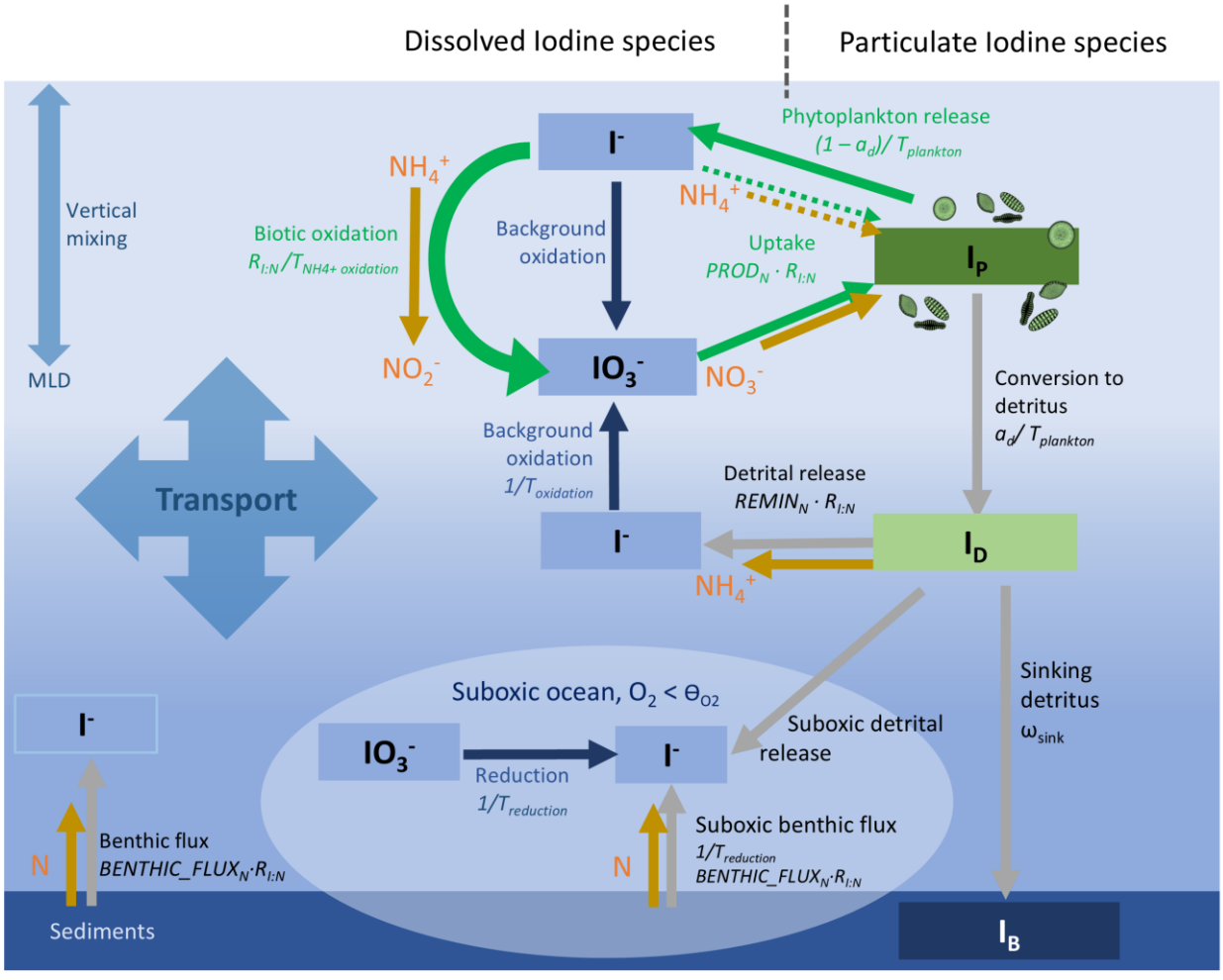

85

Figure 1: Schematic diagram of I-CYCLE model scheme, showing state variables, key processes and model parameters. Dissolved iodine reservoirs are shown on the left, and particulate reservoirs on the right. See Table 1 for description of model variables and Table 2 for model parameters. Brown arrows indicate nitrogen fluxes that certain iodine transformations are coupled to.

https://doi.org/10.5194/egusphere-2026-4580
Preprint. Discussion started: 7 September 2026

2 Model description

The iodine reservoirs and transformations in the I-CYCLE model, along with the processes they are coupled to are summarised in Fig. 1 and described in the following sections. The iodine cycling model is driven by the offline physical and biogeochemical forcing fields obtained from UKESM 1.0, as listed in Table 1 (Sect. 2.1 and 2.2). State variables are introduced in Sect. 2.3 and the tendency terms that act on them are described in Sect. 2.4. The functional form and parameterisation of the terms within the equations is then described in Sect. 2.5, and their reasons for inclusion and development discussed. Optimised model parameters under the final model configuration are listed in Table 2. The I-CYCLE model is written in Matlab and the final version of the model code is available via Zenodo (Chance et al., 2026).

2.1 The physical ocean framework

The I-CYCLE model is a global model and, unlike that of Wadley et al. (2020), extends through the entire water column. It uses a nominally 1° tri-polar grid in the horizontal with enhanced equatorial resolution (eORCA1), as used in UKESM 1.0 (Kulbrodt et al., 2018; Sellar et al., 2019). This facilitates the use of forcing fields obtained from UKESM 1.0. The 75 depth levels available in UKESM 1.0 are combined into 15 bundles of five levels each (Table S1). This constitutes a significant increase in depth resolution compared to the three-layer model of Wadley et al. (2020).

Physical forcing fields describing advection and mixing (Table 1) are obtained from UKESM 1.0 (Sellar et al., 2019). These use the Nucleus for European Modelling of the Ocean framework (NEMO; Madec et al., 2016), which incorporates an ocean general circulation model and a separate sea-ice model. Use of these forcing fields allows for spatial variation in vertical and horizontal mixing to be accounted for, whereas in the previous model (Wadley et al., 2020) advection was governed by horizontal currents (with fixed diffusivity co-efficients) taken from the OCCAM general circulation model.

2.2 Biogeochemical forcing fields

UKESM 1.0 incorporates the Model of Ecosystem Dynamics, nutrient Utilisation, Sequestration and Acidification (MEDUSA-2.1) biogeochemical model (Yool et al., 2013), and we use components of this to drive iodine transformations. This represents a substantial change from our previous model (Wadley et al., 2020), which used a satellite derived primary productivity climatology and an off-line model derived nitrification rate to drive iodide formation and loss respectively. MEDUSA includes two types of phytoplankton (diatoms and non-diatoms), two types of zooplankton (micro- and meso-), together with sinking detritus and sediment reservoirs, and the oceans are treated as a closed, conservative system without riverine inputs. The base currency of the MEDUSA model is nitrogen; the input variables and rates used to drive iodine transformations in I-CYCLE are listed in Table 1. Iodine fluxes are coupled to nitrogen fluxes using I:N ratios (see Sect. 2.4), whereas the previous model linked fluxes using a spatially variable, sea surface temperature dependent I:C ratio (extended to an I:N ratio by assuming

https://doi.org/10.5194/egusphere-2026-4580
Preprint. Discussion started: 7 September 2026

Redfield C:N stoichiometry of 106:16 for nitrification linked processes). The use of biogeochemical forcing fields from MEDUSA 2.1 rather than satellite products avoids the need to make simplistic assumptions about primary productivity where observational data is not available.

While the I-CYCLE model is embedded within the UKESM framework, it is not interactive and does not feed back to the UKESM. As iodine is not a limiting micronutrient in the oceans and is not known to significantly impact the biogeochemical cycles of other major elements, and the UKESM atmospheric module does not include iodine chemistry, this lack of feedback is expected to have a negligible effect on ocean iodine.

2.3 State variables in I-CYCLE

The prognostic variables in the I-CYCLE model are listed in Table 1. As in Wadley et al. (2020), these include concentrations of the two major dissolved forms of iodine (I^- and IO_3^-). These two ions make up the majority of the marine iodine inventory, with a total concentration of around 450 to 500 nM in most regions of the ocean, and their interconversion is the dominant feature of the marine iodine cycle (Wong, 1991; Elderfield and Truesdale, 1980). In oxygenated waters, iodide is elevated in the mixed layer, with highest concentrations observed at lower latitudes and in coastal waters, reaching up to ~50% of total dissolved inorganic iodine (Wong, 1991; Chance et al., 2014). Below the mixed layer, iodide concentrations tend to be very low (<10 nM). In anoxic basins and strong ODZs, all dissolved iodine may be present as iodide. Trends in iodate concentrations are broadly the inverse of those in iodide (Chance et al., 2014). Dissolved organic iodine (DOI) is typically a minor dissolved iodine fraction in seawater (< 5-10%; Wong and Cheng, 1998; Huang et al., 2005; Jones et al., 2024; Streanga et al., 2024) and is not included explicitly in the I-CYCLE model. As it is a reduced form of iodine, DOI can be considered to be accounted for within the iodide reservoir of the model.

Particulate iodine reservoirs were absent from our earlier model Wadley et al. (2020) but are now included. These are iodine associated with phytoplankton (I_P), sinking detritus (I_D) and the benthic layer (I_B). Observations of particulate iodine (equivalent to I_P and I_D combined) indicate it is typically present at concentrations of less than 1 nM (<0.2% of total iodine), with highest concentrations found in the euphotic zone (Wong et al., 1976; Jickells et al., 1990; Satoh et al., 2023). As well as acting as an iodine store, the detrital iodine reservoir provides a route by which iodine may be transported from the near surface to depth and potentially be incorporated into sediments on the sea floor. Sediments can be an iodine source (Tsunogai, 1971; Ullman and Aller, 1985; Wong and Zhang, 2003; Cutter et al., 2018) and inclusion of the benthic iodine reservoir allows these fluxes to be simulated.

In addition to iodine reservoirs, the model formulation requires the speciation of nutrient nitrogen to be estimated. Therefore, a tracer ('F_{NH4}') which specifies the fraction of dissolved nitrogen present as ammonium is also calculated by I-CYCLE (see Sect. 2.5.8).

https://doi.org/10.5194/egusphere-2026-4580
Preprint. Discussion started: 7 September 2026

Table 1: State variables in the I-CYCLE model and input variables and rates taken from UKESM 1.0

Symbol	Variable	Unit	Dimensionality
Variables in I-CYCLE			
I^-	Iodide concentration	mol I m^{-3}	3D
IO_3^-	Iodate concentration	mol I m^{-3}	3D
I_P	Iodine in (Phyto)plankton concentration	mol I m^{-3}	3D
I_D	Detrital iodine concentration	mol I m^{-3}	3D
I_B	Benthic iodine concentration	mol I m^{-2}	2D
F_{NH4}	Ammonium fraction of nutrient nitrogen	n/a	3D
Input variables and rates from UKESM 1.0			
N	Nutrient nitrogen	mol N m^{-3}	3D
N_D	Nitrogen in sinking detritus	mol N m^{-3}	3D
N_B	Benthic nitrogen	mol N m^{-2}	2D
$PROD_N$	Sum of diatom and non-diatom primary production, expressed as phytoplankton nitrogen uptake rate	mol N m^{-3} s^{-1}	3D
$REMIN_N$	Nitrogen remineralisation rate	mol N m^{-3} s^{-1}	3D
$BENTHIC\ FLUX_N$	Nitrogen flux out of sediment	mol N m^{-2} s^{-1}	2D
O_2	Dissolved oxygen	µmol kg^{-1}	3D
MLD	Mixed layer depth	m	2D
uo, vo	Horizontal velocities	m s^{-1}	3D
wfo	Freshwater flux into the ocean	m s^{-1}	2D

https://doi.org/10.5194/egusphere-2026-4580
Preprint. Discussion started: 7 September 2026

2.4 Differential equations

Concentrations of iodine species at a given point in space and time are a function of both physical advection and mixing (grouped together as '*TRANSPORT*' here), and production and loss by various biogeochemical processes (Eq.s 1 to 5). These equations combine the processes shown in Fig. 1 for each variable. Dissolved iodine species are taken up by phytoplankton ('*UPTAKE*') and either released again as iodide ('$RELEASE_{phytoplankton}$') or transferred to the detrital reservoir ('*EXPORT*'). Note uptake of iodide to phytoplankton ('$UPTAKE_{I^-}$'; Eq. 1 and Eq. 3) was an optional process that was evaluated during method development, but was set to zero in the final, optimised version of the model and only iodate uptake was allowed (see Sect. 2.5.2). The detrital reservoir sinks through the water column ('*SINKING*'), releasing iodide as it does so via remineralisation ('$RELEASE_{detrital}$'). Any detrital iodine reaching the sea floor is incorporated into the benthic reservoir, which itself supplies iodide to the ocean ('*BENTHIC FLUX*'). Iodide is converted to iodate by oxidation, either in parallel with biologically mediated ammonium (NH_4^+) oxidation ('$OXIDATION_{biotic}$') and/or by an independent process ('$OXIDATION_{background}$'). Some terms only operate in suboxic waters, defined by a set oxygen threshold. These are direct reduction of iodate to iodide ('$REDUCTION_{suboxic}$'), and release from detritus and benthic sediments under reducing conditions ('$RELEASE_{suboxic\ detrital}$' and '$BENTHIC\ FLUX_{suboxic}$' respectively). The equations are stepped forward in time using a leapfrog scheme with a timestep of 45 minutes and the physical and biogeochemical forcing fields are updated monthly.

$$\frac{\partial[I^-]}{\partial t} = TRANSPORT - (UPTAKE_{I^-}) + RELEASE_{phytoplankton} + RELEASE_{detrital} + BENTHIC\ FLUX - OXIDATION_{biotic} - OXIDATION_{background} + REDUCTION_{suboxic} + RELEASE_{suboxic\ detrital} + BENTHIC\ FLUX_{suboxic} \quad (1)$$

$$\frac{\partial[IO_3^-]}{\partial t} = TRANSPORT - UPTAKE_{IO3^-} + OXIDATION_{biotic} + OXIDATION_{background} - REDUCTION_{suboxic} \quad (2)$$

$$\frac{\partial[I_P]}{\partial t} = TRANSPORT + (UPTAKE_{I^-}) + UPTAKE_{IO3^-} - RELEASE_{phytoplankton} - EXPORT \quad (3)$$

$$\frac{\partial[I_D]}{\partial t} = TRANSPORT + SINKING + EXPORT - RELEASE_{detrital} - RELEASE_{suboxic\ detrital} \quad (4)$$

$$\frac{\partial[I_B]}{\partial t} = SINKING - BENTHIC\ FLUX - BENTHIC\ FLUX_{suboxic} \quad (5)$$

https://doi.org/10.5194/egusphere-2026-4580
Preprint. Discussion started: 7 September 2026

2.5. Interaction functional forms

In this section we describe the functional form of the terms within equations 1 to 5 above and discuss their development and rationale. The model was developed iteratively, with different approaches to the representation of iodine transformations evaluated at each stage by comparison with available observations. Observations were taken from an augmented version of the sea surface iodide database (Chance et al., 2019; see Table S2 for details). Note the number of iodide observations used to constrain I-CYCLE was more than three times higher than used for development of Wadley et al., 2020 (n = 4774 vs 1342 previously) and in addition, iodate observations (n = 5130) were also used. Model development particularly focused on two key points of uncertainty:

1. Whether dissolved iodine is taken up by phytoplankton "accidentally" in parallel with nitrogen, or whether it behaves like a nutrient and is taken up at a biologically "preferred" ratio to nitrogen. Evaluation of these options is discussed in Sect. 2.5.2.
2. How best to represent iodide oxidation and the extent to which it is coupled to biological ammonium oxidation. Approaches used to simulate iodide oxidation are discussed in Sect. 2.5.6.

In addition, new representations of suboxic processes have been implemented (Sect. 2.5.7). Once the final model configuration was decided, ensemble runs were undertaken to optimise parameter choices (Sect. 2.5.9); values that yielded closest agreement between observations and model output are listed in Table 2.

2.5.1 Transport and mixing

For each prognostic variable (represented here by *T)*, '*TRANSPORT*" is the sum of the advective and diffusive transports in vertical and horizontal directions (Eq. (6)), expressed in Cartesian form here for clarity,

$$TRANSPORT = -\left(\frac{\partial(uT)}{\partial x} + \frac{\partial(vT)}{\partial y} + \frac{\partial(wT)}{\partial z}\right) + A_h\left(\frac{\partial^2 T}{\partial x^2} + \frac{\partial^2 T}{\partial y^2}\right) + K_z\frac{\partial^2 T}{\partial z^2}, \quad (6)$$

where u, v, w are the zonal, meridional and vertical velocities, A_h is the horizontal diffusivity and K_z is the vertical diffusivity. Advection uses monthly mean UKESM 1.0 velocities. The variables within the mixed layer are instantaneously mixed over the UKESM 1.0 monthly mixed layer depth (MLD) at each time step. Detritus is also subject to vertical sinking (Sect. 2.5.4).

2.5.2 Dissolved iodine uptake to phytoplankton

In I-CYCLE, the action of phytoplankton on dissolved iodine species is initiated by uptake to the phytoplankton reservoir (I_P). While it is not yet confirmed whether biologically mediated iodate reduction is assimilatory or dissimilatory, iodine is considered to be a biophilic element and the small depletion of total dissolved iodine in the euphotic zone suggests uptake

https://doi.org/10.5194/egusphere-2026-4580
Preprint. Discussion started: 7 September 2026

occurs (Elderfield and Truesdale, 1980; Wong, 1991). Laboratory culture studies using radiotracers have demonstrated iodine assimilation by phytoplankton (Moisan et al., 1994; de la Questa and Manley, 2009), and other studies have reported a lag between decreases in iodate concentrations and increases in iodide, consistent with either uptake to phytoplankton cells or transformation via some other intermediate reservoir such as DOI (Chance et al., 2007; Bluhm et al., 2010). The I-CYCLE approach contrasts with our earlier model (Wadley et al., 2020), in which dissolved iodate was directly converted to dissolved iodide at a rate that was proportional to primary productivity, but explicit uptake of iodine was not included.

To parameterise this process, iodine uptake is coupled to nitrogen uptake ('$PROD_N$') using an I:N ratio R (Eq.s (7) and (8)). As field and laboratory observations show biologically mediated iodate depletion from the dissolved phase (e.g. Campos et al., 1996; Chance et al., 2007; Chance et al., 2010; Bluhm et al., 2010) we assume that iodate is the species taken up, and that - as proposed by Wong (Wong 2001; Wong and Hung, 2001) - this uptake is coupled to nitrate (NO_3^-) uptake ('$PROD_{NO3-}$'; Eq. (7)). Given the similarities in structure and redox state between iodate and nitrate ions, it is biochemically plausible that these ions are taken up in parallel. Similarly, Cheng et al. (2024) include the assimilation of iodate by phytoplankton in association with photosynthesis in their model. Despite the widely observed iodate depletion in the euphotic zone associated with primary production, it has been suggested that iodide is the biologically preferred form of iodide for phytoplankton to take up (de la Questa and Manley, 2009). Therefore, during model development stages, also allowing iodide uptake was explored. Consistent with the redox states of the two species, iodide uptake was assumed to be linked to ammonium uptake ($PROD_{NH4+}$'; Eq. (8)). However, developmental ensemble members allowing iodide uptake had lower skill (with regard to simulating observations) than those with only iodate uptake, and so iodide uptake is excluded from the final model formulation (i.e. Eq. (8) is set to zero).

$$UPTAKE_{IO3-} = PROD_{NO3-} \cdot min\left(\frac{[IO_3]}{[NO_3]}, R_{max}\right) \cdot a_I \quad (7)$$

$$UPTAKE_{I-} = PROD_{NH4+} \cdot min\left(\frac{[I^-]}{[NH_4]}, R_{ox}\right) \cdot a_I \quad (8)$$

The derivation of speciated nitrogen uptake required to drive Eq.s (7) and (8) is described in Sect. 2.5.8. Where the total iodine uptake (Eq.s (7) and (8) summed) over a given time step (Δt) is greater than the available iodate, uptake is scaled by that ratio (a_I; Eq. (9)). In practice, with only iodate uptake allowed, this prevents uptake of iodate exceeding the total amount available. If iodide uptake is also allowed, this has the effect of slowing all iodine uptake as iodate becomes depleted.

$$a_I = min\left(\frac{[IO_3^-]}{(UPTAKE_{IO3-} + UPTAKE_{I-}) \cdot 2\Delta t}, 1\right) \quad (9)$$

https://doi.org/10.5194/egusphere-2026-4580
Preprint. Discussion started: 7 September 2026

As noted earlier, a key question addressed during model development was whether dissolved iodine is taken up by phytoplankton "accidentally" in parallel with nitrogen (i.e. at the ambient seawater I:N ratio), or whether it behaves like a trace nutrient and is taken up at a biologically "preferred" ratio to nitrogen. It has not been confirmed whether phytoplankton require iodine as a micronutrient. Given the sufficiency of iodine in the marine environment, it is not thought to limit growth in the oceans, and although some algae species have been found to grow in nominally iodine-free culture media, the presence of trace concentrations of iodine species as contaminants of other salts cannot be ruled out (van Bergeijk et al., 2016). Iodine has been implicated in the oxidative stress response and defence mechanisms of macroalgae (Kupper et al., 2008) and may serve a similar role in phytoplankton. Thus, it remains an open question as to whether iodine is assimilated by phytoplankton as a micro-nutrient, or it just passively cycles with other elements. This has a profound impact on how iodine might behave in relation to nitrogen: if it is a micronutrient, its uptake is expected to be linked to carbon fixation, and by extension (using a Redfield ratio approach) to nitrogen uptake, at a biologically preferred I:C:N ratio, while if it is taken up passively the I:N uptake ratio will be dictated by the relative concentrations of dissolved iodine and nitrogen species in the surrounding seawater. The iodine cycling model of Wadley et al. (2020) used a prescribed I:C (and hence I:N) ratio, consistent with iodine being a micro-nutrient. However, it was necessary to vary this ratio with SST to obtain a fit between observed and model iodine speciation and the reasons for this variation could not be elucidated. Hence the previous model does not enlighten us as to which iodine uptake scenario is most plausible, and they are explored here.

Mathematically, "accidental" uptake can be represented by simply multiplying the N uptake rate by the seawater concentration ratio (i.e. replacing the min term in Eq.s (7) and (8) with the seawater concentration ratio alone), while uptake at a "preferred" ratio can be represented by use of the minimum term in equations (7) and (8) and specifying a maximum I:N uptake ratio. Initial iterations of the model used the former approach. However, this yielded implausibly high iodate to nitrate uptake ratios (approaching 10) in regions with strong nitrate depletion such as the Atlantic that were associated with excessively low iodate and high surface iodide concentrations. This suggests that the concept of 'accidental' uptake of iodate may only be valid for 'low' ambient I:N ratios (around 0.01 to 0.1). Where ambient seawater I:N ratios exceed such values, it may be necessary to constrain them to simulate realistic iodine uptake rates. Therefore, in the second model formulation, new parameters were introduced which limit the I:N ratios for iodine uptake by phytoplankton (and also the coupling of ammonium and iodide oxidation; Sect. 2.5.6). This approach is more similar to that taken in Wadley et al., 2020. However, we now use a globally universal preferred I:N ratio, rather than one that varies as a function of temperature as was used previously. We assume that where dissolved iodine is depleted and the seawater I:N ratio drops below the preferred value, uptake will take place at the lower, environmentally determined ratio. Over the course of model development, a wide range of maximum I:N values (0.001 to 0.33, equivalent to 1 x 10^{-4} to 0.05 I:C assuming Redfield stoichiometry) were explored, with the parameter space of subsequent model iterations converging around values at the lower end. The optimised I:N ratio under the final model configuration was 0.002 (Table 2), which is in good agreement with previous empirical and model estimates (Sect. 3.1).

https://doi.org/10.5194/egusphere-2026-4580
Preprint. Discussion started: 7 September 2026

2.5.3 Fate of phytoplankton iodine

Iodine is lost from the phytoplankton reservoir by two processes: some is released back to seawater as iodide ('$RELEASE_{phytoplankton}$'; Eq. (10)) through processes such as exudation, cell lysis and sloppy feeding, while the remaining fraction (a_d) is converted to detrital iodine (I_D) through processes such as cell death and incorporation into faecal pellets via zooplankton grazing and egestion (Eq. (11)). The overall rate of iodine loss from the planktonic pool is defined by a fixed lifetime, $T_{plankton}$.

$$RELEASE_{phytoplankton} = \frac{(1 - a_d) \cdot [I_P]}{T_{plankton}} \quad (10)$$

$$EXPORT = \frac{a_d \cdot [I_P]}{T_{plankton}} \quad (11)$$

These processes are a more explicit representation of the conversion of iodate to iodide in conjunction with primary production than implemented in Wadley et al., 2020. Release of iodide from the plankton reservoir (Eq. (10)) simulates the biologically mediated reduction of iodate to iodide in the surface ocean and allows for a proportion of iodide release to be decoupled from the nitrogen remineralisation, as is thought to be the case in the water column (Truesdale, 1994). This approach differs from that in Cheng et al. (2024), where all iodide release from particulate organic matter is coupled to remineralisation.

2.5.4 Iodine loss from detritus to seawater

The inclusion of a detrital iodine reservoir allows for iodine to be transported via sinking as well as by advection and mixing. This process provides a route for iodide release at greater depths, and can also supply iodine to the sedimentary reservoir, both of which were absent from the earlier model (Wadley et al., 2020). The sinking of I_D through the water column is described by Eq. (12), where the velocity (ω_{sink}) is 2.5 m day^{-1} (Yool et al., 2013).

$$SINKING = \omega_{sink} \cdot \frac{\partial [I_d]}{\partial z} \quad (12)$$

As detritus sinks, it breaks down and iodine is released back to the dissolved phase as iodide. This release is quantified as the nitrogen flux from detrital remineralisation ('$REMIN_N$') multiplied by the ratio of iodine to nitrogen within the detritus (Eq. (13)). This mechanism of iodide formation is analogous to the reduction of iodate to iodide via the biological pump in Cheng et al., 2024.

$$RELEASE_{detritus} = min\left(REMIN_N \cdot min\left(\frac{[I_D]}{[N_D]}, R_{max}\right), \frac{[I_D]}{2\Delta t}\right) \quad (13)$$

https://doi.org/10.5194/egusphere-2026-4580
Preprint. Discussion started: 7 September 2026

As for iodine uptake, a min term allows the detrital I:N ratio to be capped at a set maximum ratio, which is taken to be the same as that used for iodate uptake to phytoplankton (R_{max}). The amount of iodine released from detritus is limited to that available for a given timestep. Any remaining detrital iodine that reaches the sea floor is incorporated into the benthic (i.e. sediment) iodine reservoir (I_B).

2.5.5 Benthic iodine fluxes

Observations of elevated iodide concentrations in proximity to the sea floor suggest iodide may be released from sediments, especially under reducing conditions (Tsunogai, 1971; Ullman and Aller, 1985; Wong and Zhang, 2003). This flux is simulated in I-CYCLE by scaling the benthic nitrogen outbound flux ($BENTHIC\ FLUX_N$) by an I:N ratio (Eq. (14)).

$$BENTHIC\ FLUX\ = BENTHIC\ FLUX_N\ \cdot min\left(\frac{[I_B]}{[N_B]}, R_{max}\right) \quad (14)$$

As elsewhere, min terms are used to specify the I:N ratio to be used. This is the smaller of the environmental I:N ratio (i.e. the iodine:nitrogen ratio in the benthic layer), or a preset maximum ratio which is taken to be the same as that for iodate uptake (R_{max}). The 2D benthic iodide flux is divided by the thickness of the deepest ocean layer to convert it into a concentration change. To the best of our knowledge, sedimentary iodine fluxes were not included in either of the previous iodine models.

2.5.6 Iodide oxidation

To maintain the apparent steady state in iodide and iodate concentrations, iodide must be oxidised to iodate in the water column. Rates of this process are not well constrained: mass balance based estimates range from ~8 to 560 nM yr^{-1}, while recent incubation studies suggest rates of up to 189 nM yr^{-1} (Campos et al., 1996; He et al., 2013; Hardisty et al., 2020; Schnur et al., 2024). The mechanism is unknown but presumed to be biologically mediated. Water column observations have suggested iodide oxidation may be related to nitrification processes (Truesdale et al., 2001; Žic et al., 2013) and a study using laboratory cultures demonstrated it could be brought about by ammonium oxidising bacteria (Hughes et al., 2020). Consequently, iodide oxidation was explicitly linked to nitrification in the earlier model of Wadley et al., 2020. However, further evidence linking iodide oxidation and nitrification has not yet emerged and a recent laboratory study suggests that ammonium oxidising archaea, which are widespread and abundant nitrifiers, may not oxidise iodide (Webb et al., 2025). Therefore, approaches to parameterising iodide oxidation were revisited during development of the I-CYCLE model.

Specifically, iodide oxidation was either directly coupled to ammonium oxidation ('$OXIDATION_{NH4+}$'; Eq. (15)), and/or took place independently via first order kinetics according to a defined lifetime (i.e. $1/k$, referred to as $T_{oxidation}$; Eq. (16)). For simplicity, the former is referred to as 'biotic' oxidation ($OXIDATION_{biotic}$), and the latter as 'abiotic' or 'background' oxidation

https://doi.org/10.5194/egusphere-2026-4580
Preprint. Discussion started: 7 September 2026

($OXIDATION_{background}$), though it is acknowledged that the latter may be influenced by unknown biological processes (Luther, 2023). As for iodine uptake, the ratio used to scale biotic iodide and ammonium oxidation rates is the lesser of the ambient iodide:ammonium seawater ratio and a predetermined upper limit (R_{ox}). The rate of ammonium oxidation itself is given in Sect. 2.5.8 (Eq. (22)). Both iodide oxidation pathways are assumed to only occur in oxic waters (i.e. $O_2 \geq$ threshold).

$$OXIDATION_{biotic} = OXIDATION_{NH4+}(z) \cdot min\left(\frac{[I^-]}{[NH_4^+]}, R_{ox}\right) \quad (15)$$

$$OXIDATION_{background} = \frac{[I^-]}{T_{oxidation}} \quad (16)$$

During early stages of model development, iodide oxidation was restricted to a single process. At first, only biotic iodide oxidation (Eq. (15) was included, as this approach gave the best agreement between modelled and observed iodine fields in our earlier model (Wadley et al., 2020). However, when this was allowed to occur at seawater I:N ratios in I-CYCLE, iodide oxidation was rapid and simulated iodide concentrations were too low, even when using parameter options that maximise iodide concentrations. It was concluded that assuming iodide oxidation takes place in conjunction with ammonium oxidation at an environmentally determined I:N ratio is not tenable. We next explored implementing abiotic iodide oxidation (Eq. (16)) alone, with lifetimes between 0.5 and 8 years. However, this also gave unsatisfactory results. Specifically, all lifetimes resulted in surface (< 100 m depth) iodide concentrations being too high, indicating insufficient oxidation, but the shortest lifetime also oxidised too much iodide at depth, resulting in lower concentrations than observed below 100 m. Cheng et al. (2024) also compared schemes in which iodide oxidation is linked to assumed rates of ammonia oxidation (indirectly via the impact of bacterial activity on oxygen levels) with a first order iodide oxidation scheme similar to that in Eq. (16). They found that both approaches yielded comparable results, which is consistent with our finding that neither single representation of iodide oxidation gave notably better performance than the other.

As neither oxidation mechanism alone yielded good agreement with observations, subsequent iterations of the model allowed iodide oxidation to take place by both biotic (Eq. (15)) and abiotic (Eq. (16)) pathways operating in parallel. In addition, a maximum 'preferred' I:N ratio was specified for the biotic pathway. Development ensembles explored under this formulation indicated that to both reproduce the observed vertical distribution of iodide and allow extensive ODZ derived iodide plumes such as those reported in the Pacific, oxidation rates must decrease with depth. This is consistent with rates of carbon turnover and associated bacterial activity generally being higher in the surface ocean than at depth. It was achieved in the model by varying ammonia oxidation rates in a manner consistent with observations (see Sect. 2.5.8). Meanwhile, it is assumed that the rate of background iodide oxidation is constant throughout the ocean. In the final model configuration, slow background iodide oxidation (lifetime 160 years; Sect. 2.5.9) is combined with biotic iodide oxidation driven by a depth dependent ammonium

https://doi.org/10.5194/egusphere-2026-4580
Preprint. Discussion started: 7 September 2026

oxidation rate (Fig. S1; Sect. 2.5.8). The maximum I:N ratio for the latter (R_{ox})was set to be the same as that for iodine uptake; in practice this must be approximately the case for production and loss fluxes of iodide to be balanced in the ocean interior. Total iodide oxidation is the sum of these two processes.

2.5.7 Suboxic iodine transformations

A major disadvantage of our earlier model (Wadley et al., 2020) was the exclusion of processes impacting iodine speciation and abundance in suboxic regions of the oceans. Elevated iodide and low iodate concentrations are observed in ODZs, especially the Arabian Sea (Farrenkopf and Luther, 2002), the Eastern Tropical North Pacific (ETNP; Moriyasu et al., 2020) and the Eastern Tropical South Pacific (ETSP; Cutter et al., 2018), and anoxic basins (Wong and Brewer, 1977) and are primarily attributed to in situ iodate reduction. In ODZs the main driver of this reaction is likely to be the use of iodate as a terminal electron acceptor in anaerobic bacterial respiration (dissimilatory reduction; Farrenkopf et al., 1997; Amachi et al., 2007; Reyes-Umana et al., 2022). Abiotic reactions with reducing metals ($Mn2^{+}$, Fe^{2+}) may also take place (Councell et al., 1997; Luther, 2023). Under euxinic conditions, iodate is rapidly reduced by sulfide (Zhang and Whitfield, 1986; Luther, 2023). Sedimentary iodide fluxes leading to total dissolved iodine concentrations well above the global baseline level of 450 to 500 nM (referred to as 'excess iodine') have also been reported in these environments (Cutter et al., 2018; Farrenkopf and Luther, 2002; Moriyasu et al., 2020). As well as having a profound impact on iodine speciation locally, this iodide formation and sedimentary release may impact dissolved iodine speciation beyond low oxygen zones as a result of the long lifetime of iodide with respect to oxidation. Observations suggest elevated iodide concentrations arising from low oxygen waters at depth may even reach the ocean surface (Cutter et al., 2018; Chance and Tinel et al., 2020) and thus have potential to impact air-sea exchange processes. Therefore, in a substantial advance from the previous model of Wadley et al. (2020), the I-CYCLE model includes key suboxic processes, namely water column iodate reduction and detrital and benthic iodide release.

We define a universal dissolved oxygen threshold (θ_{O2}) below which these suboxic processes take place. During model development, a range of values informed by the literature were explored leading to a final optimised threshold of 7 μmol kg^{-1} (Table 2). A similar threshold approach was taken in iodine models using cGENIE (Lu et al. 2018; Cheng et al., 2024). However, we acknowledge that in reality the relationship between iodate depletion and oxygen level in suboxic waters is complex and spatially variable (Hardisty et al., 2021).

Suboxic iodate reduction in the water column is represented using a defined lifetime ($T_{reduction} = 1/k$; Equation 17). Following the findings of Farrenkopf et al. (1997), first order kinetics are assumed. Within ODZs, iodide maxima are often coincident with secondary nitrite maxima, suggesting iodate reduction may be associated with the reduction of nitrate (denitrification) and consistent with their comparable ability to act as an electron acceptor i.e. similar redox potentials. (Farrenkopf and Luther, 2002; Moriyasu et al., 2020). Consequently, we use the same lifetime for suboxic nitrate reduction as for iodate reduction (see later, Equation 23).

https://doi.org/10.5194/egusphere-2026-4580
Preprint. Discussion started: 7 September 2026

$$REDUCTION_{suboxic} = \frac{[IO_3]}{T_{reduction}} \quad (17)$$

In suboxic waters, detrital iodine (I_D) is also converted to dissolved iodide. The suboxic release of iodine from detritus in the model occurs simultaneously and instantaneously (over a timestep), whereby all iodine in I_D at a given timestep is transferred to iodide (Eq. (18)):

$$RELEASE_{suboxic\ detrital} = \frac{I_D}{2\Delta t} \quad (18)$$

Enhanced release of iodide from sediments under suboxic conditions is thought to be responsible for large plumes of 'excess' iodide associated with some ODZs, especially the ETSP (Farrenkopf and Luther, 2002; Cutter et al., 2018). Iodate is known to be retained in sediments more strongly than iodide (Price and Calvert, 1973; Ullman and Aller, 1985; Wong and Zhang, 2003), so reduction of benthic iodine in suboxic conditions may be responsible for these higher fluxes. To account for this phenomenon in the model, where dissolved oxygen concentrations fall below the suboxic threshold, an additional benthic iodine flux is included. This is simulated by reducing the benthic iodine reservoir using the same lifetime as for water column reduction, and transferring all iodine reduced by this to the overlying water (Eq. (19)).

$$BENTHIC\ FLUX_{suboxic} = N_B \cdot min\left(\frac{[I_B]}{[N_B]}, R_{max}\right) \cdot \frac{1}{T_{reduction}} \quad (19)$$

As previously (Sect. 2.5.5), the benthic iodide flux is multiplied by an extra factor of level thickness to convert the 2D flux into a concentration.

2.5.8 Introducing nitrogen speciation

In order to explicitly link iodate and nitrate uptake (Eq. (7)), and when used iodide and ammonium uptake (Eq. (8)), as well as to couple iodide oxidation to ammonium oxidation (Eq. (15)), separate tracers for nitrate and ammonium are required. UKESM 1.0 (MEDUSA) output does not include speciation of dissolved nitrogen (only total nutrient nitrogen), therefore we introduce a simplistic scheme to separate dissolved nitrogen into nitrate and ammonium. The ammonium concentration ($[NH_4^+]$) is calculated from dissolved nitrogen concentration ([N]) from UKESM using the variable F_{NH4} (Table 1) according to Eq. 20:

$$[NH_4^+] = F_{NH4+} \cdot [N] \quad (20)$$

https://doi.org/10.5194/egusphere-2026-4580
Preprint. Discussion started: 7 September 2026

The tendency term for F_{NH4} is given in Eq. (21) below:

$$\frac{\partial F_{NH4+}}{\partial t} = TRANSPORT - \frac{PROD_{NH4+} - OXIDATION_{NH4+} + REDUCTION_{NO3-} + REMIN_N}{[N]} \quad (21)$$

It is presumed that all nitrogen remineralised from organic matter ('$REMIN_N$') is as ammonium (Yool et al., 2007). Loss of ammonium by oxidation to nitrite ('$OXIDATION_{NH4+}$') is described by Eq. (22) and is considered to only take place in oxygenated waters. In order to evaluate Eq. (21) and parameterise ammonium uptake (see below), a scenario was assumed in which ammonium oxidation occurs at a prescribed lifetime ($T_{NH4+\ oxidation}$) of 5 days (Yool et al., 2007).

$$OXIDATION_{NH4+}(z) = \frac{[NH4]}{T_{NH4+\ oxidation}(z)} \quad (22)$$

Nitrate reduction ('$REDUCTION_{NO3-}$'; Eq. (23)) is assumed to only take place in suboxic waters and to have the same lifetime as for suboxic iodate reduction (Sect. 2.5.7).

$$REDUCTION_{NO3-} = \frac{[NO3]}{T_{reduction}} \quad (23)$$

We initially assumed that all nitrogen uptake is as ammonium where it is available, with nitrate uptake only taking place once ammonium has been depleted to zero. However, simulations using this assumption resulted in the complete removal of ammonium in parts of the upper ocean, and a theoretical f-ratio (the fraction of primary productivity driven by nitrate) distribution that was inconsistent with observations (Laws et al 2000). We therefore implemented a somewhat more realistic scheme where as ammonium is depleted, an increasing proportion of nitrogen uptake is as nitrate. To describe this, a weighting factor (W) is applied to the seawater concentrations of ammonium and nitrate to estimate the fraction of nitrogen uptake that is as ammonium (Eq. (24)):

$$\frac{PROD_{NH4+}}{PROD_N} = \frac{W \cdot [NH_4^+]}{(W \cdot [NH_4^+] + [NO_3^-])} \quad (24)$$

This fraction is multiplied by $PROD_N$ to obtain $PROD_{NH4+}$ by phytoplankton (Eq. (25)). The remainder of productivity is assumed to be driven by nitrate (Eq. (26)). A limit function is applied to both equations to restrict nutrient uptake to that available for a given time step.

https://doi.org/10.5194/egusphere-2026-4580
Preprint. Discussion started: 7 September 2026

$$PROD_{NH4+} = min\left(\frac{PROD_N \cdot [NH4] \cdot W}{[NH4] \cdot W + [NO3]}, \frac{[NH4]}{2\Delta t}\right) \quad (25)$$

$$PROD_{NO3-} = min\left(PROD_N - PROD_{NH4+}, \frac{[NO3]}{2\Delta t}\right) \quad (26)$$

A value of W=0 gives no ammonium uptake while W=infinity gives only ammonium uptake. Where $W \sim [NO_3] / [NH_4]$, there is a smooth transition between ammonium and nitrate uptake as ammonium becomes depleted. It was found that for W=8000 this transition resulted in an f-ratio distribution that broadly reflects that observed in the ocean (Laws et al 2000), with a value of around 0.4 in the Southern Ocean and North Atlantic, and 0.1 in the subtropical gyres.

During early stages of I-CYCLE model development, an ammonium oxidation lifetime ($T_{NH4\ oxidation}$) of 5 years was retained, but in later development a wider range of ammonium oxidation lifetimes were explored. Specifically, it appeared that improved parameterisation of iodide oxidation could be achieved by allowing ammonium oxidation lifetime to increase with depth (Sect. 2.5.6). This is consistent with observations of decreasing ammonium oxidation rate with depth, which has been identified as a trend in a recent global compilation of nitrification rates (Tang et al., 2023). To parameterise this depth dependence, an ensemble of 512 model runs was configured with eight different ammonium oxidation lifetimes for the surface, eight lifetimes for deep waters, and eight depth scales for the transition between the surface and deep. For each model level (Table S1) the ammonium oxidation lifetime that yielded iodide concentrations closest to observations was determined. This is found to increase from 140 days at 20 m to ~1000 years in the deep ocean. Results were used to create an optimal vertical profile for ammonium oxidation lifetime which is used to drive I-CYCLE (Fig. S1).

2.5.9. Optimised parameters under final configuration

Once the final configuration of I-CYCLE was decided, two model ensembles were used to determine optimum parameter values. These developmental model runs were initialised using quasi-observational iodide and iodate fields, which were created by binning observed concentrations (Table S2) into the biogeochemical provinces defined by Longhurst et al. (1998). All other variables, including other iodine reservoirs (I_P, I_D and I_B) and the ammonium fraction (F_{NH4+}) were set to zero initially. Each ensemble was run for 100 years.

As the suboxic parameters (θ_{O2}, $T_{reduction}$) are subject to considerable uncertainty and have the greatest impact in the Pacific Ocean, we first evaluated parameters that are not exclusive to suboxic processes in an ensemble that excluded the Pacific. Specifically, these runs used a range of values for R_{max}, $T_{plankton}$, a_d, R_{ox} and $T_{oxidation}$, and the values that gave best fit between observed and modelled iodide and iodate fields were identified. An ensemble of global runs with a range of values for the

https://doi.org/10.5194/egusphere-2026-4580
Preprint. Discussion started: 7 September 2026

495 dissolved oxygen threshold (θ_{O2}) and suboxic reduction lifetime ($T_{reduction}$) was then used to determine the best-fit values for these two remaining parameters. Final best-fit parameters are shown in Table 2 and their plausibility with regard to observations is discussed in Sect. 3.1.2.

Table 2: Optimised final model parameters found to give best fit to observations and consistent with values in the literature.

Symbol	Parameter	Eq.(s)	Value	Section
W	Weighting for ammonium uptake	24, 25	8000	2.5.8
$UPTAKE_{I^-}$	Uptake of iodide to phytoplankton in parallel with ammonium	8	OFF	2.5.2
R_{max}	Maximum I:N ratio for iodate uptake, and detrital and benthic iodide release	7, 13, 14	0.002	2.5.2
a_d	Plankton to detritus iodide fraction,	10, 11	0.03	2.5.3
$T_{plankton}$	Plankton iodine loss lifetime	10, 11	7 days	2.5.3
$T_{NH4+\ oxidation}$	Ammonium oxidation lifetime	15, 22	Vertical profile (Fig. S1)	2.5.6, 2.5.8
R_{ox}	Maximum I:N ratio for biotic iodide oxidation ratio (also used for iodide uptake when allowed)	15, (8)	0.002	2.5.6
$T_{oxidation}$	Background iodide oxidation lifetime,	16	160 years	2.5.6
$T_{reduction}$	Iodate reduction and benthic release lifetime where suboxic; also used as nitrate reduction lifetime where suboxic	17, 23	8 years	2.5.7
θ_{O2}	Dissolved oxygen threshold for suboxia	Condition	7 µmol kg^{-1}	2.5.7

500

2.6 Model simulations

For production runs, the I-CYCLE model was initialised using variable fields taken from the end (year 100, month 12) of the optimisation ensemble run that contained the best-fit parameters (Sect. 2.5.9). This is equivalent to a 100-year pre-industrial

https://doi.org/10.5194/egusphere-2026-4580
Preprint. Discussion started: 7 September 2026

spin-up. It was run for a further 150 years (1850 to 2099) using the best fit parameters (Table 2) under (1) pre-industrial control conditions, and (2) a changing climate, using scenarios taken from UKESM 1.0 (Tang et al., 2019; Good et al., 2019). The changing climate run (2) ran from historical (1850-2014) through to future (2015-2099) under the SSP585 scenario. The control run (1) confirmed that model drift was minimal and resulted in negligible changes compared to those under a changing climate (2). To smooth out inter-annual fluctuations such as El Niño events, iodine fields are represented by 20-year climatologies for the time periods of interest.

3. Results and Discussion

In this section we present iodide and iodate fields generated by the I-CYCLE model in its final, optimised configuration and consider model credibility and performance. The model is first evaluated in terms of the plausibility of the best-fit parameter values (Sect. 3.1), and then by comparison of present-day fields with observations (Sect. 3.2). Present day output is also compared to that from the earlier model (Wadley et al., 2020) and the most widely used sea surface iodide parameterisations (Sect. 3.3). Finally, we present simulated iodide and iodate fields for 2100 (Sect. 3.4).

3.1 Plausibility of model parameters

In addition to reproducing observations, the credibility of I-CYCLE as a representation of the marine iodine cycle can be evaluated by considering the plausibility of the best-fit parameter values that were determined through tuning the model to best fit observations (R_{max}, a_d, $T_{Plankton}$, $T_{oxidation}$, θ_{O2}, $T_{reduction}$).

The best-fit I:N value (R_{max}) was 0.002 mol mol^{-1}, with the same ratio applied to both iodine uptake and iodide oxidation (Table 2). Assuming Redfield stoichiometry (i.e. C:N ratio of 106:16), this corresponds to an I:C uptake ratio of 3 x 10^{-4}. This is very similar to observation-based estimates of the I:C ratio of biologically mediated iodate removal (and/or iodide formation) to carbon fixation, which range from 1.6 x 10^{-4} to 6.4 x 10^{-3} (Campos et al., 1996; Chance et al., 2010). It is slightly higher than measurements of the I:C content of particulate organic matter (1 x 10^{-4}; Elderfield and Truesdale, 1980; 1 to 5 x 10^{-5}, Satoh et al., 2023), which is reasonable given that a portion of the iodine taken up is rapidly released back to the dissolved phase. It is also very similar to the model best-fit value of 1.5 x 10^{-4} reported by Cheng et al. (2024). In contrast, in the earlier model of Wadley et al., model best fit was achieved by decreasing the I:C ratio from 3 x 10^{-4} to 3.8 x 10^{-5} (equivalent to I:N ratios from 0.002 to 0.0003) going from low to high sea surface temperatures. That the I:C ratios required by the two models should only agree in low temperature waters is consistent with the difference in the formulation of iodate uptake, which is associated with *all* nitrogen uptake in Wadley et al. (2020) but only nitrate uptake in I-CYCLE. In colder waters, nitrate tends to be the dominant driver of primary production, meaning iodine uptake is coupled to a similar nitrogen flux under both model formulations and so might reasonably be governed by a similar I:N ratio. Meanwhile in warmer waters, ammonium is the dominant form of nitrogen taken up - as this is not associated with iodine uptake in I-CYCLE, this results in lower iodine

https://doi.org/10.5194/egusphere-2026-4580
Preprint. Discussion started: 7 September 2026

uptake without changing the I:N ratio, whereas in the earlier model the I:N uptake ratio must be decreased to achieve the same effect.

The best-fit value for the proportion of phytoplankton iodine transferred to sinking detritus (a_d) was 0.03 (Table 2). Significant deviations from this value were found to produce excessive or insufficient iodide at mid depths in the model. The value is strikingly similar to the percentage of assimilated iodine that observations suggest reach the ocean interior (3%; Wong et al. 1976).

The best-fit lifetime for the release of iodine from plankton ($T_{plankton}$) was found to be 7 days, but the difference in performance was small and the model was essentially insensitive to values ranging from 7 to 120 days. The existence of a lag supports the involvement of an intermediate iodine reservoir (in this case phytoplankton cells) in the reduction of iodate to iodide. Given that individual phytoplankton lifetimes are of the order of a few days (Marba et al., 2007), a 7-day lifetime is broadly consistent with evidence from laboratory cultures which suggests iodide release is associated with cell senescence (Bluhm et al., 2010; Hepach et al., 2020).

There is considerable uncertainty over the rate of iodide oxidation ($T_{oxidation}$) in the oceans, with lifetime estimates ranging from ~70 days to 50 years (Campos et al., 1996; Hardisty et al., 2020; Cheng et al., 2024). Observations suggest rates may be more rapid above the mixed layer than below, with additional mechanisms operating in surface waters (Campos et al., 1996; Moriyasu et al., 2023). This is conceptually similar to the way oxidation rates are represented in I-CYCLE. Our best-fit background iodide oxidation lifetime of 160 years is longer than the slowest literature estimates (40 to 50 years; Tsunogai, 1971; Lu et al., 2018; Cheng et al., 2024). However, these estimates are for total iodide oxidation, whereas in our model 'background' iodide oxidation is in addition to 'biotic' oxidation, and so the overall lifetime with respect to oxidation will be considerably shorter. The formulation for 'biotic' oxidation implies a very wide range of rates; in eutrophic surface waters where ammonium is extremely high, iodide lifetimes with respect to 'biotic' oxidation may be less than a year, but elsewhere they will range from tens to 1000s of years dependent on relative ammonium and iodide concentrations.

The oxygen threshold (θ_{O2}) below which suboxic iodate reduction takes place has been estimated as 20 to 70 µmol kg^{-1} from measurements of foraminiferal iodine:calcium ratios (Lu et al., 2016). Initial estimates of this value made using the cGENIE model were within this range, at 30 µmol kg^{-1} but were lowered in the most recent iteration of that model to 10 µmol kg^{-1} (Lu et al., 2018; Cheng et al., 2024). In the modern ocean, a universal oxygen threshold below which iodate is consistently depleted has not been identified, but iodate depletion (< 150 nM) in ODZs typically only occurs where oxygen is below 7 µmol kg^{-1} (Hardisty et al., 2021). In I-CYCLE the optimal value for the oxygen threshold below which suboxic transformations are

https://doi.org/10.5194/egusphere-2026-4580
Preprint. Discussion started: 7 September 2026

initiated was 7 μmol kg^{-1} (Table 2). Given the very good agreement with the lower thresholds identified by Cheng et al. and Hardisty et al., and the uncertainty in observational constraints, we consider our value to be reasonable.

Our best-fit lifetime for suboxic iodate reduction ($T_{reduction}$) was 8 years (Table 2), which is equivalent to a first order rate constant (as per Eq. 17) of 0.34 x 10^{-3} day^{-1}. This is much slower than early observations of extremely rapid iodate reduction (lifetimes of ~0.15 days or less) in samples collected from the Arabian Sea ODZ (Farrenkopf et al., 1997). However subsequent observations suggest rates of suboxic iodate reduction are highly heterogeneous through the water column and between ODZ regions. In incubation experiments conducted in the ETNP, iodate reduction was only detectable in samples collected from the upper oxycline, where the first order rate constant was reported as >0.56 d^{-1}, corresponding to a lifetime of <1.78 days (Hardisty et al., 2021). This is much faster than our value, but at other depths including the ODZ core, iodate reduction was not detectable and minimum lifetimes with respect to oxidation were at least 7 to 16 days (Hardisty et al., 2021). Rates may be even slower in other locations such as the ETSP, where iodate concentrations greater than 150 nM persist despite oxygen being undetectable (Cutter et al., 2018; Hardisty et al., 2021). As we apply a universal reduction lifetime across all suboxic waters, our longer lifetime may reflect averaging across a small volume of waters with rapid reduction and larger volumes with much slower reduction.

3.2 Present day ocean iodine distribution

3.2.1 Sea surface iodide and iodate

Simulated annual average iodide and iodate concentrations for the ocean surface layer (2.9 ± 2.9 m depth) are shown in Fig. 2, and latitudinally averaged values are shown alongside observations in Fig. 3. Across most latitudes, simulated values fall within the envelope of concentrations observed globally at that parallel (Fig. 3a). I-CYCLE replicates key features of the observed sea surface iodide distribution that have been identified previously (Chance et al., 2014), most notably the large-scale trend of increasing iodide with decreasing latitude across the sub-tropics with a dip around the equator (Fig. 3a). In general, the distribution of iodate is the opposite to that of iodide (Fig. 2), congruent with transformations between these two species being the dominant feature of the marine iodine cycle.

https://doi.org/10.5194/egusphere-2026-4580
Preprint. Discussion started: 7 September 2026

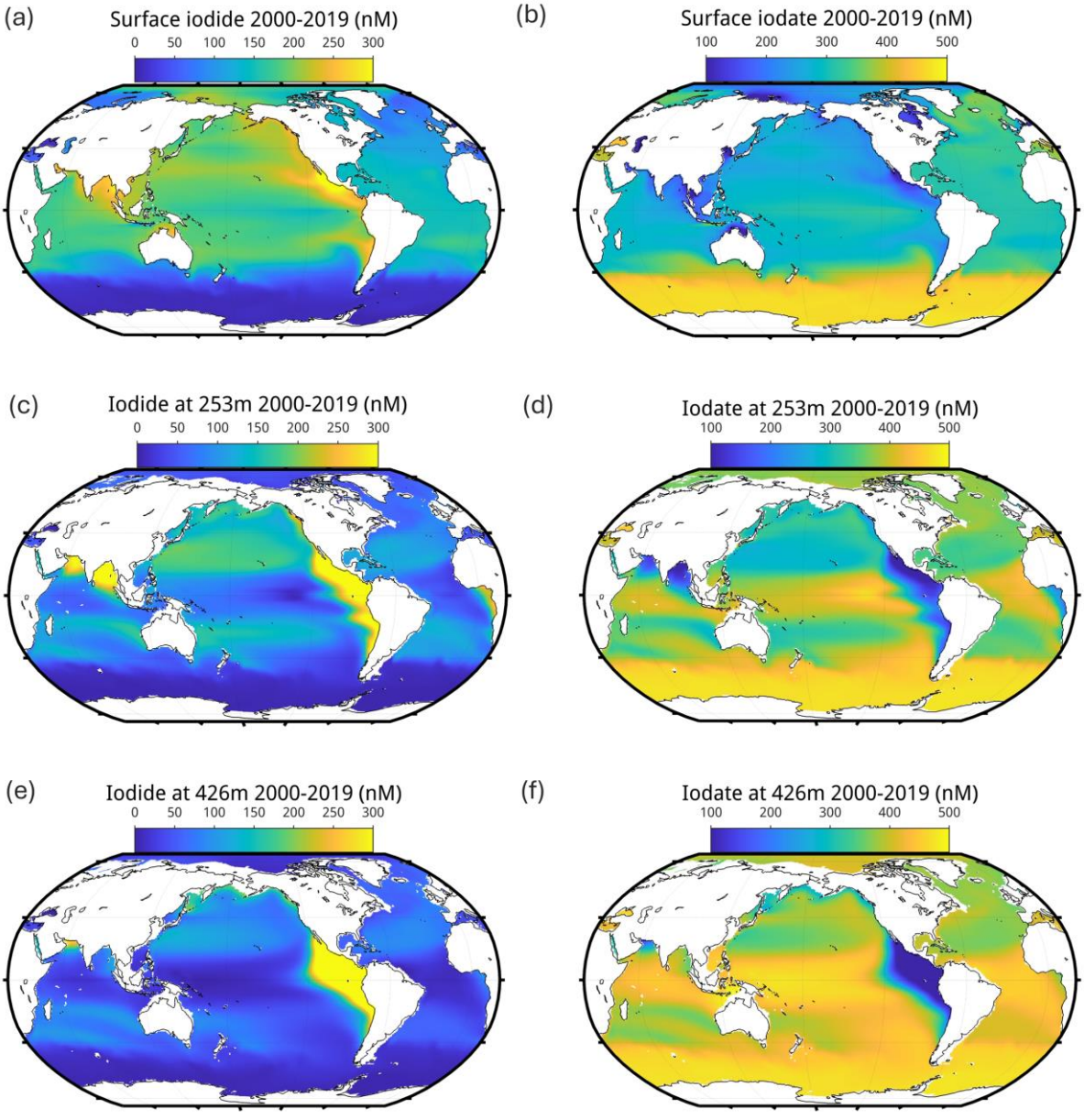

595

Figure 2: Present day (2000-2019) annual mean iodide (a,c,e) and iodate (b,d,f) concentrations simulated by the I-CYCLE model with optimised parameters run under the 'historical-SSP585 scenario' from 1850 after 100 years of model spin-up, for (a,b) surface (2.9 ± 2.9 m), (b,d) 253 ± 63.5 m, and (e,f) 426 ± 109.5 m depth layers.

https://doi.org/10.5194/egusphere-2026-4580
Preprint. Discussion started: 7 September 2026

The overall performance of the I-CYCLE model may be quantified by comparison of simulated iodide and iodate concentrations with observations. Considering only sea surface concentrations (model surface layer vs. observations from <25 m depth), this yields root mean square errors (RMSEs) of 119 (Table 3) and 101 nM for iodide and iodate respectively. The model has a moderate positive bias for surface iodide (normalised mean bias (NMB) of 0.2; Table 3), but not for iodate (NMB of 0.0004). Although the model has been tuned against observations, these overall average errors are large relative to typical ambient concentrations (<250 nM). Model error will arise not only from limitations in our representation of the iodine cycle, but also from the skill of UKESM to simulate accurate physical and biogeochemical forcing fields. In addition, these errors likely reflect the scarcity observations (n = 1351 for iodide and 1201 for iodate) combined with their large range (2.5 to 2039 nM for iodide, 0 to 582 nM for iodate) and known interannual variability (e.g. Chance et al., 2010).

https://doi.org/10.5194/egusphere-2026-4580
Preprint. Discussion started: 7 September 2026

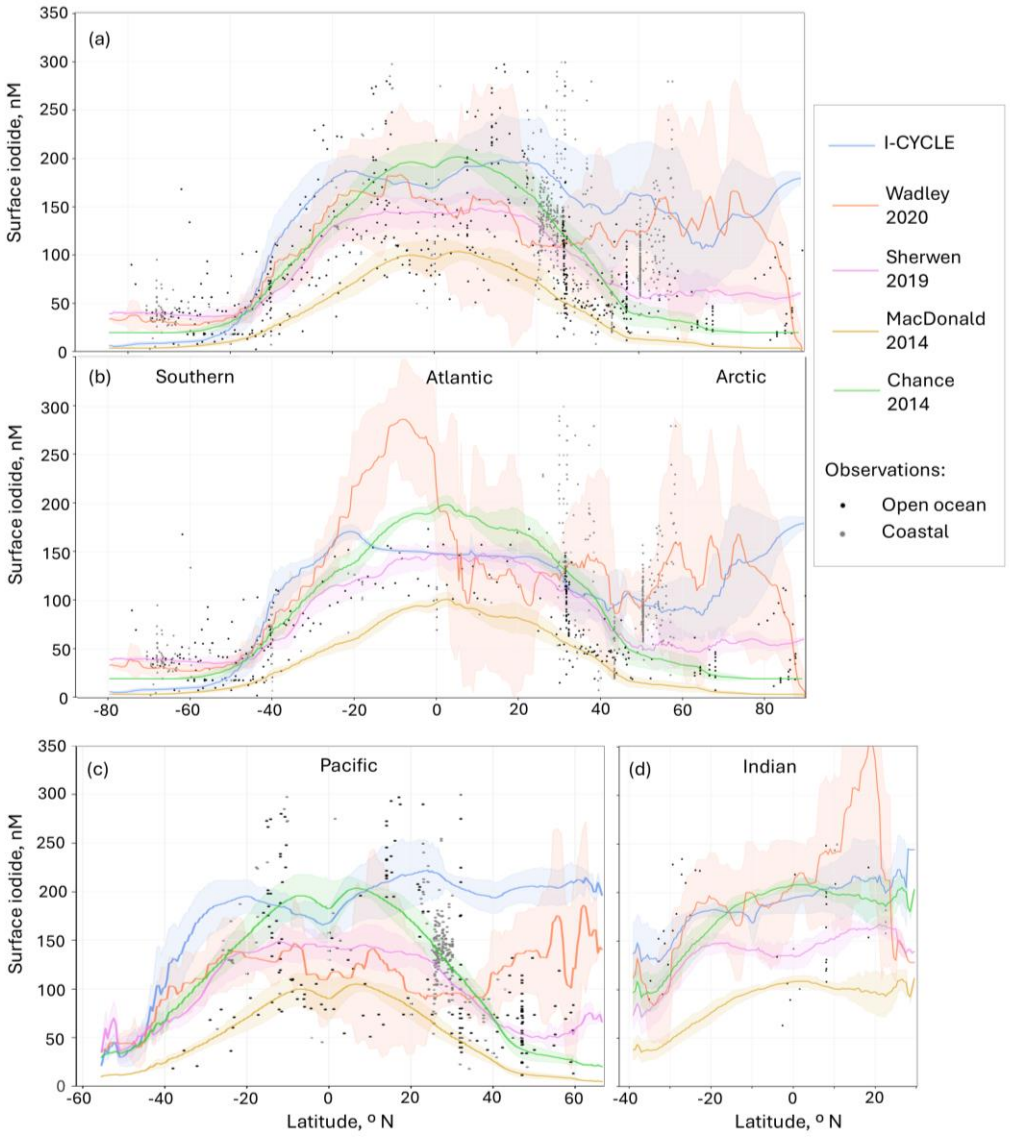

Figure 3: Variation of sea surface iodide concentrations with latitude for the global ocean (a), and the Atlantic, Arctic and Southern Oceans (b), the Indian Ocean (c), and the Pacific Ocean (d). Observations are shown as dots, with grey indicating coastal locations and black for the open ocean. Continuous lines show simulated concentrations generated by I-CYCLE (blue), Wadley et al., 2020 (red), Sherwen et al., 2019 (magenta), MacDonald et al., 2014 (yellow), and Chance et al., 2014 (green).

Model performance varies geographically, with best performance (i.e. smallest difference between observed and modelled values) for sea surface iodide found in the Atlantic, Indian and Southern Oceans, as well as the Mediterranean and central

https://doi.org/10.5194/egusphere-2026-4580
Preprint. Discussion started: 7 September 2026

Pacific (Fig. 4b). Simulated concentrations in the Atlantic follow latitudinal trends in observations (Fig. 3b). There is a small asymmetry, with slightly higher concentrations in the southern subtropical Atlantic than the north (Fig. 3b), likely arising from the influence of African eastern boundary upwelling systems (EBUS). A pronounced concentration gradient is simulated at the boundary of the Southern Ocean (Fig. 2a; Fig. 3a and 3b), in agreement with observations of very low sea surface iodide concentrations at high southern latitudes and distinct shifts as ocean fronts are crossed (Fig. 4; Campos et al., 1999; Bluhm et al., 2011; Chance and Tinel et al., 2020).

High iodide concentrations (>250 nM) are simulated in Pacific EBUS and plumes of elevated iodide extend westwards across the Pacific from these regions (Fig. 2a), broadly consistent with reports of high surface iodide associated with these systems (Fig. 4; Cutter et al., 2018; Moriyasu et al., 2020). Similarly, relatively high sea surface iodide concentrations are predicted in the northern Indian Ocean (Arabian Sea and the Bay of Bengal; Fig. 2a; Fig. 3d), where high iodide concentrations have been observed (Fig. 3d & 4; Farrenkopf and Luther, 2002; Chance and Tinel et al., 2020; Shaikh et al., 2024). The eastern Pacific and Arabian Sea have very high biological productivity (Antoine et al., 1996) and exhibit particularly strong correlations between modelled iodide and primary productivity (Fig. S4), suggesting this is a key driver of elevated iodide in these regions. Strong stratification in areas such as the Bay of Bengal (Prasanna Kumar et al., 2002) may further contribute to high iodide at the ocean surface. However, the plumes of elevated iodide that stretch across the sub-tropical north and south Pacific do not correspond with the more equatorial plume in primary production (Antoine et al., 1996) or areas of shallower mixed layer depth (Montegut et al., 2004), indicating an additional cause. As the high values emanate from the ODZ regions, this may be iodide supplied to the surface from subsurface iodide maxima, discussed further in Sect. 3.2.3.

The positive bias in predicted iodide concentrations is largely driven by over-prediction in the northern and western Pacific (Fig. 3c; Fig. 4b). The reasons for this have not yet been ascertained. Mixed layer depth tends to be underestimated by UKESM 1.0 in the North Pacific (Kuhlbrodt et al., 2018), which could contribute to artificially high surface iodide concentrations. UKESM 1.0 also simulates bands of dissolved oxygen below the threshold of 7 μmol kg^{-1} along the northern Pacific coast (Fig. S3) which will drive iodide accumulation in I-CYCLE but may not be realistic: UKESM 1.0 underpredicts oxygen in the North Pacific (Lee et al., 2022) and observations from the region indicate conditions that are hypoxic but above the iodate reduction threshold (Evans et al., 2024). As there is not an overall equivalent negative bias in iodate, the positive iodide bias may result from over-estimating external (i.e. benthic) iodide inputs, which are enhanced under low oxygen conditions in I-CYCLE.

https://doi.org/10.5194/egusphere-2026-4580
Preprint. Discussion started: 7 September 2026

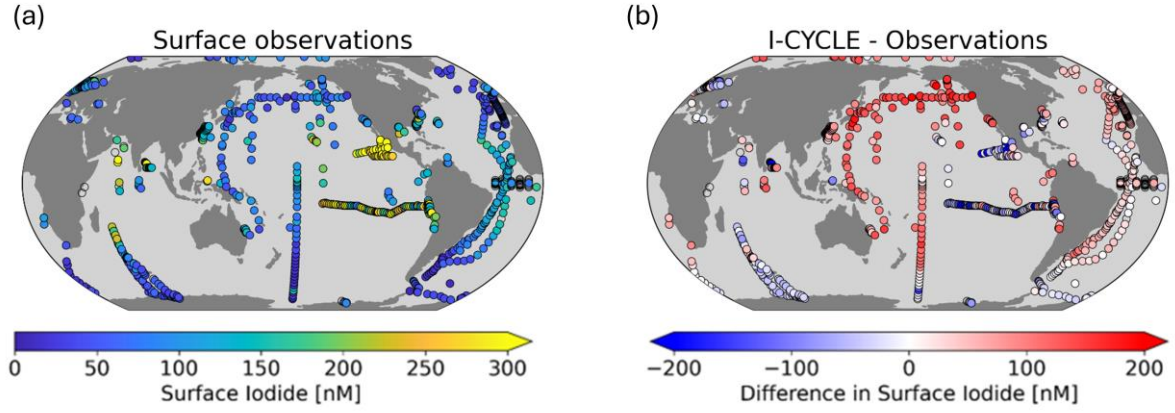

Figure 4: (a) Sea surface (< 25 m) iodide observations from the augmented Chance et al. (2019) data set, and (b) difference between annual average present day sea surface iodide concentrations simulated by I-CYCLE and these observations.

The model may also over-predict iodide in the Arctic. In contrast to the Southern Ocean and Antarctic coastal waters, I-CYCLE predicts relatively high annual surface iodide concentrations in the Arctic (Fig. 2a, Fig. 3b). This difference may be driven by the Arctic having weaker vertical mixing and higher biological productivity than the Southern Ocean. In previous attempts to model iodine speciation, Arctic predictions were subject to particularly high uncertainty due to an almost complete lack of available observations at the time (Sherwen et al., 2019; Wadley et al., 2020). Arctic observations reported since then suggest iodide may indeed be relatively high in northern polar waters, with sea surface iodide concentrations of 76 to 113 nM measured in the high Arctic in late summer (Zhang et al., 2023). However, I-CYCLE predictions are higher still than this (Fig. 4b). Marine iodine emissions may be especially important in the Arctic, as iodine has been implicated in new particle formation in the clean Arctic atmosphere (Baccarini et al., 2020). Further observations are urgently needed to better understand the distribution and controls on iodine speciation in this climate critical and rapidly changing region.

3.2.2 Iodide and iodate in the oxygenated ocean interior

In oxygenated waters, iodate is the dominant species below the mixed layer (Chance et al., 2014). The I-CYCLE model broadly replicates expected depth distributions of iodide and iodate, with lower iodide and higher iodate concentrations at depth compared to the surface across most of the oceans (Fig. 2). To further explore the ability of I-CYLE to replicate iodine speciation with depth, we consider selected locations where iodine speciation has been well studied.

At the Bermuda Atlantic Time Series Station in the subtropical Atlantic, a time series study was conducted in the 1990s (Campos et al., 1996) and the site was revisited in 2018 (Schnur et al., 2024). Surface iodide concentrations are consistently

https://doi.org/10.5194/egusphere-2026-4580
Preprint. Discussion started: 7 September 2026

high (100-150 nM) and drop off steeply to a few tens of nM through the upper 200 m, while iodate does the opposite (Fig. 5a). I-CYCLE replicates the surface values well but mean deep water iodide concentrations are over-estimated by ~10 - 20 nM and iodate under-estimated by ~50 - 80 nM. In the model output, elevated iodide concentrations also persist to greater depths (~500 - 600 m) than observed. This may be due to positive biases in UKESM 1.0 estimates of monthly MLD at this location (Kuhlbrodt et al., 2018). As this excessive downward mixing does not also result in underestimated surface iodide concentrations, by implication either iodide production must also be too high, and/or iodide loss rates too slow.

In the South Atlantic near the Antarctic convergence, sea surface iodide concentrations are much lower (~20-30 nM) but also decline with depth (Fig. 5b; Campos et al., 1999). Very similar depth profiles have been reported at comparable latitudes elsewhere (Bluhm et al., 2011). I-CYCLE replicates these profiles, but with a less pronounced vertical gradient and a slight under-estimation of iodate at depth (Fig. 5b). The under-estimation of iodate at depth here and in the subtropical Atlantic again suggests the iodide oxidation rate below the mixed layer may be too slow at these sites, which could also contribute to over-estimation of iodide at the surface (Sect. 3.2.1). This possibility is consistent with I-CYCLE iodide oxidation rates being slower than those reported in the literature (Sect. 3.1).

At a third site, near the eastern Australian continental shelf break, surface iodide concentrations are high and iodate low, as is commonly observed in coastal waters (McTaggart et al., 1994; Fig. 5c). I-CYCLE broadly replicates this, though it overestimates surface iodide by up to ~50 nM. However, as in the subtropical Atlantic, the strong concentration gradients through the upper 200 m are not replicated and iodide is over-estimated down to 500 m (Fig. 5c). As above, this may reflect over-estimation of mixed layer depth combined with iodide over-production and/or sluggish oxidation.

On a global scale, comparison of I-CYCLE output and observations below 25 m depth yields RMSE values of 161 and 104 nM for iodide and iodate respectively. The greater iodide error at depth compared to the surface (Sect. 3.2.1) likely reflects the wider concentration ranges encountered (0 to 8100 nM). The magnitude of the iodide error is greater than suggested by the differences between observed and simulated concentrations discussed above (Fig. 5). Furthermore, in the above examples iodide at depth is over-estimated, while overall I-CYCLE iodide concentrations below 25 m depth have a negative bias overall (NMB of -0.17). This implies regions of different ocean regimes are likely driving the overall negative bias in iodide predictions. Iodate at depth does not have an equivalent positive bias (NMB of -0.05), suggesting that the cause might be an under-estimation of the rate of iodide release from another reservoir, which could be sinking detrital matter or the benthic layer.

https://doi.org/10.5194/egusphere-2026-4580
Preprint. Discussion started: 7 September 2026

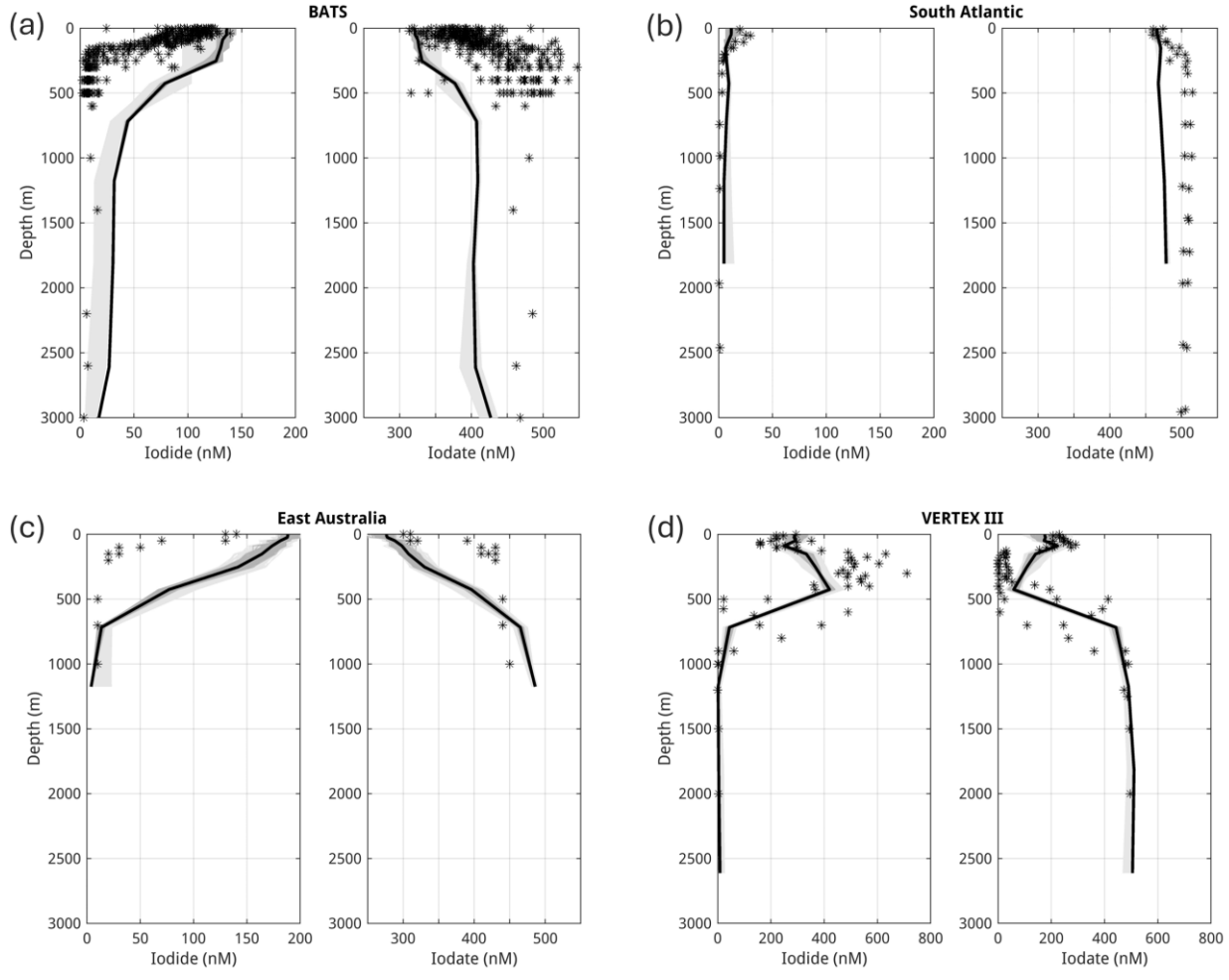

Figure 5: Present day iodide (left) and iodate (right) depth profiles simulated by I-CYCLE (continuous shading), alongside available observations (asterisks), for (a) the Bermuda Atlantic Time Series station (32°N, 64°W), (b) the South Atlantic (54°S, 35°W, (c) eastern Australian coast (24°S, 153°E), and (d) the Vertex III station in the ETNP (15°N, 107°W). Model data shows 250 years output from the control run in light grey, 20 years present day (2000-2019) in darker grey and the mean in black. Observational data taken from (a) Campos et al., 1996 and Schnur et al., 2024; (b) Campos et al., 1999; (c) McTaggart et al., 1994; (d) Rue et al., 1997 and Moriyasu et al., 2020.

3.2.3 Iodine speciation in oxygen depletion zones (ODZs)

As outlined earlier, strongly elevated iodide and depleted iodate concentrations have been observed in association with ODZs (Cutter et al., 2018; Rapp et al., 2020; Moriyasu et al., 2020; Sect. 2.5.7). Consistent with this, I-CYCLE simulates severe sub-surface iodate depletion and iodide enhancement in the eastern tropical Pacific where intense ODZs are encountered (Fig. 2c & 2d). The model output suggests these are more intense in the ETNP than the ETSP, as has been reported previously (Cutter

https://doi.org/10.5194/egusphere-2026-4580
Preprint. Discussion started: 7 September 2026

et al., 2018; Moriyasu et al., 2020). At the VERTEX III site in the ETNP, which was first studied in 1982 and revisited in 2018 (Rue et al., 1997; Moriyasu et al., 2020), observed iodide and iodate depth profiles are well replicated by the I-CYCLE model (Fig. 5d).

Elevated sub-surface iodide is also simulated in the Arabian Sea where the other major ODZ occurs (Fig. 2c), in general agreement with observations (Farrenkopf & Luther, 2002; Shaikh et al., 2023). The spatial extent of elevated iodide at 253 and 426 m in the Pacific and Arabian Sea closely agrees with areas where dissolved oxygen is predicted to be below the reduction threshold of 7 μmol kg^{-1} by UKESM 1.0 (Fig. S3). The Bay of Bengal is also a major ODZ, with a subsurface iodide maxima observed in the upper part (100-300 m; Shaikh et al., 2024). Here I-CYCLE predicts elevated iodide at 253 m but not 426 m (Fig. 2c & 2e), mirroring the depths at which UKESM 1.0 predicts low oxygen (Fig. S3). In the Atlantic, the Mauritanian and Benguela upwelling systems are not associated with such strong oxygen depletion or pronounced shifts in iodine speciation (Chapman 1983; Rapp et al., 2019; Winkelbauer et al., 2023). This is reflected in the I-CYCLE output, which simulates only modest iodide subsurface maxima at 253 m and no elevation at 426 m in the Atlantic EBUSs.

As noted earlier (Sect. 3.2.1), I-CYCLE also simulates very high surface iodide plumes that emanate from the ODZs (Fig. 2a). Observational studies suggest surface plumes of iodide arise from the subsurface ODZ and associated sedimentary sources (Cutter et al., 2018; Farrenkopf and Luther, 2002; Moriyasu et al., 2020), indicating a potential link between subsurface biogeochemical processes and atmospheric chemistry. By integrating suboxic iodine transformations with ocean transport and a plausible representation of iodide oxidation, the I-CYCLE model provides a framework to test this link.

3.3 Comparison with previous sea surface iodide models

Due to the impact of sea surface iodide on atmospheric composition (Carpenter et al., 2021), most efforts to predict marine iodine speciation have focused on iodide at the ocean surface. The earlier three layer ocean biogeochemical model of Wadley et al. (2020) only considered the upper ocean, and empirical parameterisations used by the atmospheric modelling community (MacDonald et al., 2014; Sherwen et al., 2019) are derived from iodide observations from 15 m depth or less. Here we compare I-CYCLE output for sea surface iodide (<25 m) with these previous parameterisations.

3.3.1 Comparison with previous ocean biogeochemical model

Annual average surface iodide fields from Wadley et al. (2020) were obtained from the authors and compared to the same observational data set as used to calculate RMSE for I-CYCLE. The resulting error estimate is slightly lower than achieved by the I-CYCLE model (RMSE of 112 vs 119 nM respectively; Table 3), and subject to less bias (NMB of -0.03 vs 0.20 respectively; Table 3). This indicates that the expanded depth scale, complexity and predictive power of I-CYCLE has come with a small cost to model performance.

https://doi.org/10.5194/egusphere-2026-4580
Preprint. Discussion started: 7 September 2026

Table 3: Diagnostic statistics and error estimates (root mean square error (RMSE) and normalised mean bias (NMB)) for present day (2000-2019) sea surface (<25 m) iodide fields generated using the I-CYCLE model and the climatology and parameterisations typically used to model iodide driven air-sea exchange processes. Errors are calculated against the augmented sea surface iodide database of Chance et al., 2019 (see Table S2). Sea surface temperature values used in the MacDonald et al. and Chance et al. parameterisations are taken from the same present day UKESM 1.0 fields as used to force the I-CYCLE model. *Values are for monthly data, except for Wadley et al., 2020 for which only annual average iodide fields were available and equivalent statistics for I-CYCLE.

Predictor	[Iodide], nM			Iodide errors	
	Area weighted mean	25th - 75th percentile	Maximum	RMSE, nM	NMB
This study	140.7	35.7 - 184.8	427.0	119.0 118.8*	0.2 0.2*
Wadley et al. 2020	118.9	38.40 - 150.5	720.3	112.4*	-0.03*
Sherwen et al. 2019	100.8	43.0 - 135.4	244.3	111.3	-0.2
MacDonald et al. 2014	53.3	3.9 - 71.1	237.2	136.3	-0.6
Chance et al. 2014 (Eq. 1 from Table 2)	116.1	19.8 - 159.9	4277.5	159.1	-0.09

Although both models broadly replicate the key features of the sea surface iodide distribution (Fig.s 2, 3 and 6a), comparison of these fields reveals some notable differences. I-CYCLE predicts higher concentrations in the Pacific than the earlier model (Fig. 6b), likely due to the inclusion of low oxygen processes, leading to a higher global area weighted mean concentration (Table 3). The earlier model had been revealed to under-estimate iodide in this ocean basin by observations reported after its development. Conversely, I-CYCLE predicts lower iodide than the earlier model in the Atlantic EBUS, which were previously over-estimated (Wadley et al., 2020), and also the northern Indian Ocean (Fig.s 3 and 6). Overall, there is a more pronounced difference between the Atlantic and Pacific basins in the newer model, consistent with observations. Both I-CYCLE and the earlier model predict high iodide concentrations in the Arctic relative to Antarctic waters (Fig. 3b). However, the distribution and magnitude of predicted Arctic iodide has changed such that I-CYCLE predicts higher levels across much (but not all) of the Arctic (Fig. 6b). Both models predict very similar iodide concentrations at subarctic latitudes, whereas Wadley et al. (2020) predicts lower values in the high Arctic and is in closer agreement with the few observations made there (Fig. 3b).

https://doi.org/10.5194/egusphere-2026-4580
Preprint. Discussion started: 7 September 2026

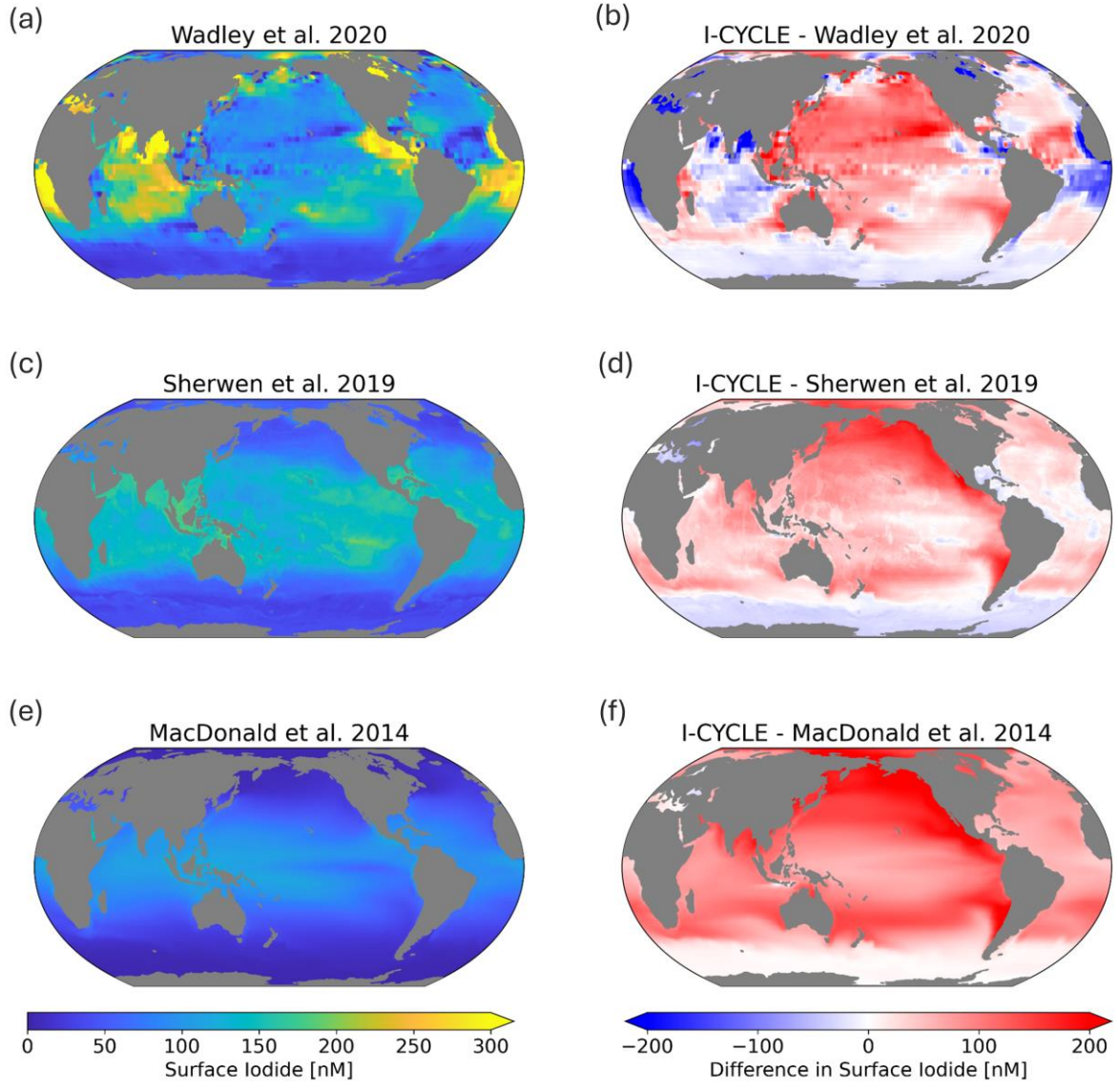

Figure 6: Comparison of annual average present day sea surface iodide concentrations simulated by I-CYCLE compared to (a,b) simulated fields from Wadley et al. 2019, (c,d) Sherwen et al., 2020, and (e,f) MacDonald et al., 2014. Left panels (a,c,e) show the comparison data set used, right panels (b,d,f) show I-CYCLE output minus the comparison data set.

https://doi.org/10.5194/egusphere-2026-4580
Preprint. Discussion started: 7 September 2026

3.3.2 Comparison with empirical parameterisations

I-CYCLE has a lower RMSE than the two sea surface temperature (SST) driven parameterisations (MacDonald et al., 2014 and Chance et al., 2014) commonly used by the atmospheric modelling community, but a higher RMSE than the more recent machine learning generated climatology (Sherwen et al., 2019) (Table 3). It predicts a higher global area-weighted mean iodide concentration than all the empirical iodide parameterisations (Table 3). Whereas the I-CYCLE model has a moderate positive bias, the MacDonald, Sherwen and Chance parameterisations have a negative bias (Table 3). In particular, the MacDonald et al. (2014) parameterisation has a strong negative bias (NMB of 0.6; Table 3) and predicts much lower iodide concentrations than other approaches (Fig. 3), possibly because of the smaller data set it was derived from. The negative bias in the Sherwen et al. climatology likely arises because high iodide observations (>309.5 nM) were excluded from its development (Sherwen et al., 2019). The Sherwen et al. (2019) climatology has the most skill at predicting present day sea surface iodide fields (lowest RMSE), albeit with a comparable (but opposite) bias to I-CYCLE. However, as this was generated using a data driven, random forest regression rather than a mechanistic model, it is unable to simulate iodine fields below the surface and lacks predictive power for the future ocean.

The I-CYCLE model allows us to investigate the relationship between sea surface iodide concentration and SST that underpins two of the parameterisations discussed above (MacDonald et al., 2014; Chance et al., 2014). These parameterisations are based on large scale empirical correlations between iodide and SST, but such analyses are limited by availability of observations and mask smaller scale spatial and temporal variability in the relationship between these two parameters. Interrogation of I-CYCLE iodide fields finds that while a positive correlation with SST is observed in many regions of the ocean, it is not ubiquitous and in other regions a strong negative correlation occurs (Fig. S5). Strong positive correlations are particularly evident in the Southern Ocean (presumably due to high amplitude seasonal cycles in SST, mixed layer depth and biological activity), while strong negative correlations are particularly evident in the North Atlantic. This highlights the limitations of using SST driven parameterisations to predict local scale variations in sea surface iodide.

3.4 The impact of global change on marine iodine speciation

3.4.1 Future projections of marine iodine speciation

Global change is manifesting in various ways in the ocean. Warming results in physical changes in ocean circulation and mixing, as well as loss of sea-ice, which all in turn impact patterns of biological productivity. Dissolved oxygen concentrations are declining, and areas of low oxygen are predicted to expand (Schmidko et al., 2017; Kwiatkowski et al., 2020). By linking the iodine cycle to forcing fields from an Earth System Model, the I-CYCLE model is capable of predicting the impact of such changes on marine iodine cycling.

https://doi.org/10.5194/egusphere-2026-4580
Preprint. Discussion started: 7 September 2026

Figure 6 shows predicted iodine speciation for 2100 generated by running I-CYCLE using forcing fields from the UKESM 1.0 under the Shared Socio-economic Pathway SSP585 scenario (see earlier for details). Under this scenario, UKESM 1.0 predicts global average SST to increase by ~5.5 °C, global average mixed layer depth to decrease by ~12 m, and global average ocean primary productivity to decline by ~15%. Meanwhile, the overall percentage of ocean water categorised as suboxic in I-CYCLE (i.e. dissolved O_2 < 7 µmol kg^{-1}) does not change significantly. Driven by these changes, I-CYCLE predicts global average surface iodide concentrations to rise by only ~2 nM to 143 nM (Table 4). This overall increase is substantially smaller than that predicted by other parameterisations (MacDonald et al., 2014; Chance et al., 2014), which suggest average iodide increases of 27 nM or more (Table 4); the difference in predictions arises because other parametrisations are based solely on SST changes and do not take account of accompanying shifts in biogeochemical processes and ocean circulation.

Table 4: Projected sea surface iodide concentrations for 1880-1899 from historical forcings and for 2080-2099 under SSP585, generated using I-CYCLE and parameterisations from the literature. Sea surface temperature values used in the MacDonald et al. and Chance et al. parameterisations are taken from the same SST projections as the I-CYCLE iodide fields.

Predictor	[Iodide], nM					
	Historical (1880-1899)			Future (2088-2099 under SSP585)		
	Area weighted mean	25th - 75th percentile	Change from present	Area weighted mean	25th - 75th percentile	Change from present
This study	139.6	36.8-184.8	-1.1	142.7	42.0-181.6	+2.0
MacDonald et al. 2014	49.7	3.7-66.6	-3.6	80.6	7.3-109.7	+27.3
Chance et al. 2014	110.8	19.8-152.9	-5.3	153.1	23.5-212.2	+37.0

The distribution of predicted changes in iodine speciation is not homogenous, and the direction of change varies with location. Surface iodide concentrations are predicted to increase (and iodate concentrations decrease) in the Southern Ocean, the North Pacific and northern sub-tropical Pacific, the North Atlantic, the Mediterranean, and lower latitude regions of the Arctic (Fig. 6a). Increased iodide in the Southern Ocean and northern Pacific may arise from intensification of primary production and remineralisation in these regions, which will increase the reduction of iodate to iodide via the biological pump. Superimposed on this, shoaling of the mixed layer in parts of these regions will enhance iodide accumulation at the ocean surface. Meanwhile, in the North Atlantic, decreases in mixed layer depth may be the dominant driver of increased surface iodide concentrations.

https://doi.org/10.5194/egusphere-2026-4580
Preprint. Discussion started: 7 September 2026

In the subsurface (426 m), similar but less pronounced changes are predicted, and in addition there are areas of intense iodide increase in the ETSP and the Bay of Bengal, but not the ETNP or Arabian Sea, where subsurface concentrations may even decline (Fig. 6b). This is broadly consistent with simulated changes in dissolved oxygen concentrations - although a global decline in subsurface concentrations is predicted by UKESM, it is not located in ODZ regions (Kwiatkowski et al., 2020) whereas iodine cycling in I-CYCLE will only be impacted where concentrations drop below the threshold value of 7 µmol kg^{-1}. Future changes to ODZs are uncertain, with some studies suggesting expansion (e.g. Stramma et al., 2008) and others suggesting redistribution of hypoxic and suboxic waters (e.g. Busecke et al., 2022), but are likely to have a profound impact on marine iodine speciation. A substantial increase in sub-surface iodide concentrations is also predicted in the Arctic (Fig. 6b), reflecting rapid and pronounced shifts in biogeochemical cycling and ocean dynamics in this basin.

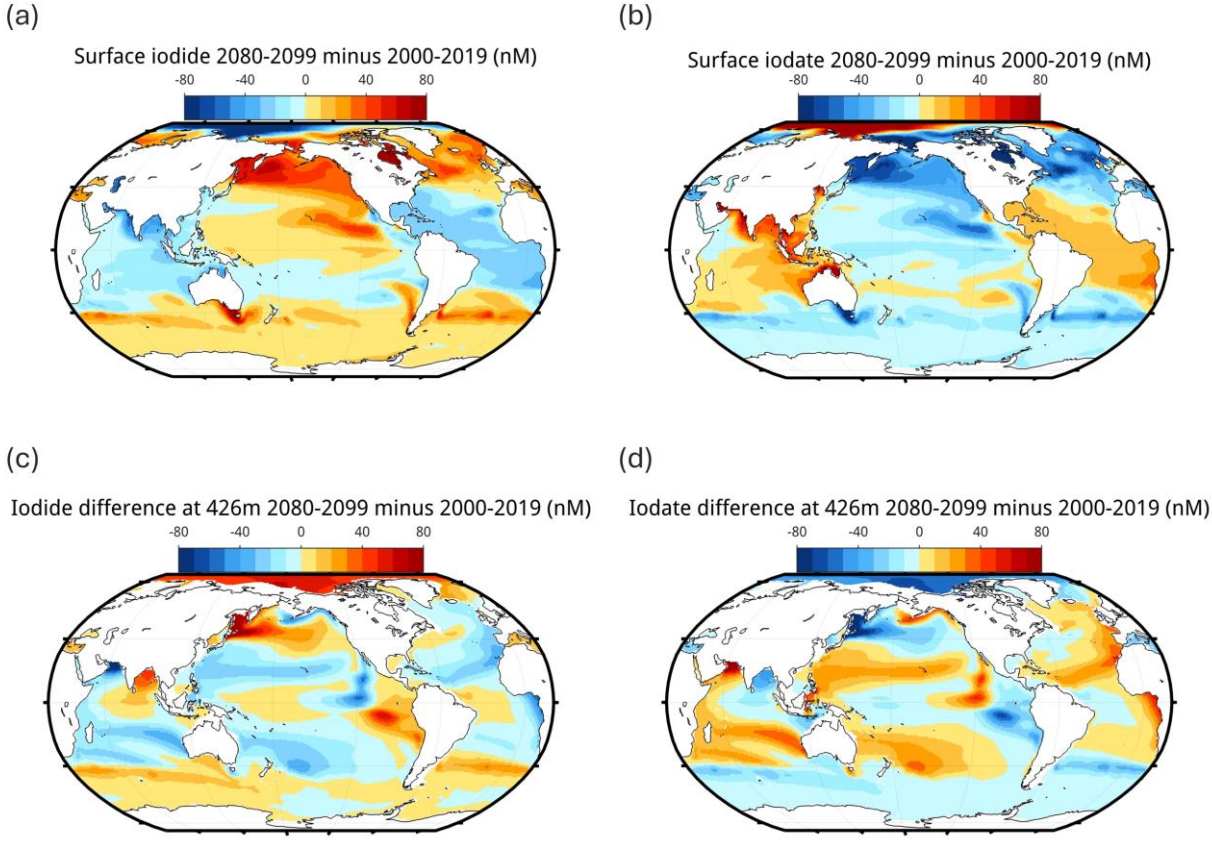

Figure 7: Changes in annual mean predicted iodide (left; a, c) and iodate (right; b, d) concentrations between present day (2000-2019) and 2080-2099 under scenario SSP585 at (a,b) surface (3 m) and (c, d) 426 m depths.

https://doi.org/10.5194/egusphere-2026-4580
Preprint. Discussion started: 7 September 2026

The previous model (Wadley et al., 2020) explored the impact on iodine speciation of ocean acidification, which may affect biological ammonium oxidation and thus iodide oxidation, by using future nitrification scenarios provided by Yool et al., 2007. The current formulation of I-CYCLE means that ocean acidification will not impact iodine cycling via changes to iodide oxidation rate in the same way. However, it would be possible to conduct sensitivity tests for this process by implementing different rates of ammonium oxidation in the model. Coastal eutrophication driven by terrestrial run-off is also changing the ocean and may impact iodine speciation. Currently such changes will not be simulated, as the oceans in UKESM 1.0 are treated as a closed system. Should perturbations in marine biogeochemical cycles caused by terrestrial run-off be included in future versions of the UKESM, I-CYCLE could capture the impacts on iodine speciation.

3.4.2 Impact of large-scale ocean oscillations

The I-CYCLE model allows the impact on iodine speciation of large-scale ocean oscillations such as El Niño–Southern Oscillation (ENSO) to be predicted. Considering December to February, when El Niño is typically most intense, sea surface iodide concentrations in the equatorial Pacific and Indian Oceans are higher by ~40 nM in El Niño years compared to La Niña years (Fig. S2). Meanwhile, iodide concentrations in the ETNP and ETSP are lower by ~ 40 nM, likely the result of enhanced upwelling of oxygen rich waters with a lower iodide signature, as was observed on the Peruvian shelf during the strong 2015 El Niño event (Rapp et al. 2020).

3.4.3 Historical sea surface iodide distributions

The I-CYCLE model may also be used to simulate historical marine iodine distributions. Marine iodine emissions are thought to have increased two- to three-fold since the pre-industrial era, largely due to increases in anthropogenic ozone (Prados-Roman et al., 2015; Cuevas et al., 2018; Legrand et al., 2018). Fully understanding these changes requires knowledge of how sea surface iodide fields have also evolved. Results from I-CYCLE suggest global average sea surface iodide concentrations were only very slightly lower (1.7 nM) at the start of the industrial period (1880-1899) than the present day (Table 4), implying that changes in iodide abundance are unlikely to have been an important driver of historical changes in iodine emissions and its subsequent deposition. Other sea surface iodide parameterisations generate similar, but slightly larger, differences between present day and pre-industrial average sea surface iodide concentrations, though the average concentrations themselves differ more markedly between approaches (Table 4).

In principle I-CYCLE could also be used to model iodine cycling in the ancient ocean, provided UKESM has been run over the relevant time period to provide appropriate forcing fields. For example, a range of paleo-experiments are being co-ordinated under the Paleoclimate Modelling Intercomparison Project, PMIP.

https://doi.org/10.5194/egusphere-2026-4580
Preprint. Discussion started: 7 September 2026

4. Concluding remarks

A new model of the marine biogeochemical iodine cycle is presented which is capable of reproducing present day global iodide and iodate distributions. While the model builds upon our previous iodine cycling model (Wadley et al., 2020), it provides a more comprehensive description of the ocean iodine cycle and a more sophisticated representation of iodine transformations. Specifically, it includes three new iodine reservoirs (phytoplankton, detrital and benthic iodine), a new approach to parameterising biological iodine uptake, and incorporates suboxic iodine transformations and sediment interactions. The inclusion of suboxic processes in the I-CYCLE model allows better representation of iodine speciation in low oxygen regions compared to the model of Wadley et al., 2020.

I-CYCLE replicates key features of the marine iodine distribution, and the optimised model parameters are consistent with values obtained in other studies. Model performance is geographically variable, and there appears to be a tendency to over-estimate iodide in some regions. In the oxygenated ocean, this may arise from under-estimation of iodide oxidation rates. Overestimation of benthic iodide inputs may also contribute to the positive iodide bias. As both these processes are poorly constrained, future refinements to their representation in I-CYCLE would benefit from more observations.

As a process-based model, I-CYCLE may be used to explore the controls on marine iodine cycling. A key question addressed during method development was whether phytoplankton take up iodine as a nutrient (i.e. at a 'preferred' ratio to nitrogen) or passively; results imply uptake behaviour between these two extremes. A second question was how best to represent iodide oxidation. In contrast to our previous work, we find that this is best done through a combination of processes, rather than assuming all iodide oxidation is directly associated with ammonium oxidation. In future work, I-CYCLE may be used to further probe the marine iodine cycle via sensitivity tests. In particular, it could be used to test the extent to which iodide arising from ODZs can reach the ocean surface (and so impact ocean chemistry) and evaluate how this may change under different ocean deoxygenation scenarios.

The I-CYCLE model is driven by outputs from UKESM 1.0, a full complexity ESM, and so can provide high resolution ocean iodine distributions for past and future climate scenarios (notwithstanding the limitations of ESMs to accurately capture Earth's climate). I-CYCLE outputs such as sea surface iodide fields are suitable for forcing atmospheric chemistry and transport models (e.g. GEOS-Chem) and so allow the impact of marine iodine cycling on atmospheric composition, and especially ozone mixing ratios, to be explored. The 2100 iodide fields generated by I-CYCLE under SSP585 have been used to assess the impact of global change on iodine driven atmospheric chemistry (Pound et al., 2026). Refinements and advances in the representation of ocean biogeochemistry and physics in the UKESM should improve the skill of I-CYCLE. For instance, implementation of speciated marine nitrogen in UKESM is likely to be an improvement on our current approach. More ambitiously, the I-CYCLE model could also be embedded within a next generation Earth System Model, with iodine species being prognostic variables.

https://doi.org/10.5194/egusphere-2026-4580
Preprint. Discussion started: 7 September 2026

https://doi.org/10.5194/egusphere-2026-4580
Preprint. Discussion started: 7 September 2026

Code and data availability

The final version of the model code and initialisation fields used in this work are available via the Zenodo repository (Chance et al., 2026; doi: 10.5281/zenodo.19697878). UKESM 1.0 data were provided by the CEDA archive (Tang et al., 2019; doi: 10.22033/ESGF/CMIP6.6298; Good et al., 2019; doi: 10.22033/ESGF/CMIP6.6405) and accessed through JASMIN (https://www.jasmin.ac.uk; Lawrence et al., 2013). Climatological I-CYCLE outputs of monthly iodide and iodate concentrations under past, present and future (SSP585) scenarios are archived at the British Oceanographic Data Centre (Wadley et al., 2026; doi: 10.5285/561a6d79-2192-7b77-e063-7086abc0ecb5)

Supplement link

Author contributions

MW developed the model with contributions from DPS, TDJ and RC. MW authored the model code and simulations were carried out by MW and DPS. Evaluation of the model was conducted by MW, RC and RJP, with formal analysis by MW, RJP and DPS. RC prepared the manuscript with contributions from MW and DPS; all co-authors contributed to review and editing of the manuscript. DPS and RJP produced manuscript figures. Funding for this work was acquired by LJC, DPS, ME and RC.

Competing interests

The authors declare that they have no conflict of interest.

Acknowledgements

Model simulations and analysis were carried out on the High-Performance Computing Cluster supported by the Research and Specialist Computing Support service at the University of East Anglia. We thank all those who have made observations of dissolved iodine species available for this work. Andrew Yool kindly uploaded some additional UKESM1 model output fields to JASMIN.

Financial support

This work was funded by the UK Natural Environment Research Council grant NE/W00027X/1(I-SEA).

https://doi.org/10.5194/egusphere-2026-4580
Preprint. Discussion started: 7 September 2026

References

Amachi, S., Kawaguchi, N., Muramatsu, Y., Tsuchiya, S., Watanabe, Y., Shinoyama, H., and Fujii, T.: Dissimilatory Iodate Reduction by Marine *Pseudomonas* sp. Strain SCT, Appl. Environ. Microbiol., 73, 5725-5730, doi:10.1128/AEM.00241-07, 2007.

Antoine, D., André, J.-M., and Morel, A.: Oceanic primary production: 2. Estimation at global scale from satellite (Coastal Zone Color Scanner) chlorophyll, Global Biogeochemical Cycles, 10, 57-69, https://doi.org/10.1029/95GB02832, 1996.

Baccarini, A., Karlsson, L., Dommen, J., Duplessis, P., Vüllers, J., Brooks, I. M., Saiz-Lopez, A., Salter, M., Tjernström, M., Baltensperger, U., Zieger, P., and Schmale, J.: Frequent new particle formation over the high Arctic pack ice by enhanced iodine emissions, Nature Communications, 11, 4924, 10.1038/s41467-020-18551-0, 2020.

Bluhm, K., Croot, P., Wuttig, K., and Lochte, K.: Transformation of iodate to iodide in marine phytoplankton driven by cell senescence, Aquat. Biol., 11, 1-15, 10.3354/ab00284, 2010.

Bluhm, K., Croot, P. L., Huhn, O., Rohardt, G., and Lochte, K.: Distribution of iodide and iodate in the Atlantic sector of the southern ocean during austral summer, Deep Sea Research Part II: Topical Studies in Oceanography, 58, 2733-2748, https://doi.org/10.1016/j.dsr2.2011.02.002, 2011.

Busecke, J. J. M., Resplandy, L., Ditkovsky, S. J., and John, J. G.: Diverging Fates of the Pacific Ocean Oxygen Minimum Zone and Its Core in a Warming World, AGU Advances, 3, e2021AV000470, https://doi.org/10.1029/2021AV000470, 2022.

Campos, M. L. A. M., Sanders, R., and Jickells, T.: The dissolved iodate and iodide distribution in the South Atlantic from the Weddell Sea to Brazil, Mar. Chem., 65, 167-175, https://doi.org/10.1016/S0304-4203(98)00094-2, 1999.

Campos, M. L. A. M., Farrenkopf, A. M., Jickells, T. D., and Luther, G. W.: A comparison of dissolved iodine cycling at the Bermuda Atlantic Time-series Station and Hawaii Ocean Time-series Station, Deep Sea Research Part II: Topical Studies in Oceanography, 43, 455-466, https://doi.org/10.1016/0967-0645(95)00100-X, 1996.

Carpenter, L. J., Chance, R. J., Sherwen, T., Adams, T. J., Ball, S. M., Evans, M. J., Hepach, H., Hollis, L. D. J., Hughes, C., Jickells, T. D., Mahajan, A., Stevens, D. P., Tinel, L., and Wadley, M. R.: Marine iodine emissions in a changing world, Proc Math Phys Eng Sci, 477, 20200824, 10.1098/rspa.2020.0824, 2021.

Chance, R., Wadley, M. R., Ryan Pound, Carpenter, L. J., Evans, M., Jickells, T., and Stevens, D. P.: I-CYCLE: v1.0.0 (Version V1.0.0) [code]. Zenodo. https://doi.org/10.5281/zenodo.19697878

Chance, R., Baker, A. R., Carpenter, L., and Jickells, T. D.: The distribution of iodide at the sea surface, Environmental Science: Processes & Impacts, 16, 1841-1859, 10.1039/c4em00139g, 2014.

Chance, R., Malin, G., Jickells, T., and Baker, A. R.: Reduction of iodate to iodide by cold water diatom cultures, Mar. Chem., 105, 169-180, https://doi.org/10.1016/j.marchem.2006.06.008, 2007.

https://doi.org/10.5194/egusphere-2026-4580
Preprint. Discussion started: 7 September 2026

Chance, R., Weston, K., Baker, A. R., Hughes, C., Malin, G., Carpenter, L., Meredith, M. P., Clarke, A., Jickells, T. D., Mann, P., and Rossetti, H.: Seasonal and interannual variation of dissolved iodine speciation at a coastal Antarctic site, Mar. Chem., 118, 171-181, https://doi.org/10.1016/j.marchem.2009.11.009, 2010.

Chance, R., Tinel, L., Sarkar, A., Sinha, A. K., Mahajan, A. S., Chacko, R., Sabu, P., Roy, R., Jickells, T. D., Stevens, D. P., Wadley, M., and Carpenter, L. J.: Surface Inorganic Iodine Speciation in the Indian and Southern Oceans From 12°N to 70°S, Frontiers in Marine Science, 7, 10.3389/fmars.2020.00621, 2020.

Chance, R. J., Tinel, L., Sherwen, T., Baker, A. R., Bell, T., Brindle, J., Campos, M. L. A. M., Croot, P., Ducklow, H., Peng, H., Hopkins, F., Hoogakker, B., Hughes, C., Jickells, T. D., Loades, D., Macaya, D. A. R., Mahajan, A. S., Malin, G., Phillips, D., Roberts, I., Roy, R., Sarkar, A., Sinha, A. K., Song, X., Winkelbauer, H., Wuttig, K., Yang, M., Peng, Z., and Carpenter, L. J.: Global sea-surface iodide observations, 1967–2018, Scientific Data, 6, 286, 10.1038/s41597-019-0288-y, 2019.

Chapman, P.: Changes in iodine speciation in the Benguela current upwelling system, Deep Sea Research Part A. Oceanographic Research Papers, 30, 1247-1259, https://doi.org/10.1016/0198-0149(83)90083-3, 1983.

Cheng, K., Ridgwell, A., and Hardisty, D. S.: Characterizing the marine iodine cycle and its relationship to ocean deoxygenation in an Earth system model, Biogeosciences, 21, 4927-4949, 10.5194/bg-21-4927-2024, 2024.

Councell, T. B., Landa, E. R., and Lovley, D. R.: Microbial reduction of iodate, Water Air Soil Pollut., 100, 99-106, 10.1023/a:1018370423790, 1997.

Cuevas, C. A., Maffezzoli, N., Corella, J. P., Spolaor, A., Vallelonga, P., Kjær, H. A., Simonsen, M., Winstrup, M., Vinther, B., Horvat, C., Fernandez, R. P., Kinnison, D., Lamarque, J.-F., Barbante, C., and Saiz-Lopez, A.: Rapid increase in atmospheric iodine levels in the North Atlantic since the mid-20th century, Nature Communications, 9, 1452, 10.1038/s41467-018-03756-1, 2018.

Cutter, G. A., Moffett, J. W., Nielsdóttir, M. C., and Sanial, V.: Multiple oxidation state trace elements in suboxic waters off Peru: In situ redox processes and advective/diffusive horizontal transport, Mar. Chem., 201, 77-89, https://doi.org/10.1016/j.marchem.2018.01.003, 2018.

de Boyer Montégut, C., Madec, G., Fischer, A. S., Lazar, A., and Iudicone, D.: Mixed layer depth over the global ocean: An examination of profile data and a profile-based climatology, Journal of Geophysical Research: Oceans, 109, https://doi.org/10.1029/2004JC002378, 2004.

de la Cuesta, J. L. and Manley, S. L.: Iodine Assimilation by Marine Diatoms and Other Phytoplankton in Nitrate-Replete Conditions, Limnology and Oceanography, 54, 1653-1664, 2009.

Elderfield, H. and Truesdale, V. W.: On the biophilic nature of iodine in seawater, Earth and Planetary Science Letters, 50, 105-114, https://doi.org/10.1016/0012-821X(80)90122-3, 1980.

Evans, N., Johnson, E., Taing, A., Schnur, A. A., Chace, P. J., Richards, S., Hardisty, D. S., and Moffett, J. W.: More Than Deoxygenation: Linking Iodate Reduction to Nitrogen, Iron, and Sulfur Chemistry in Reducing Regimes, Journal of Geophysical Research: Oceans, 129, e2024JC021013, https://doi.org/10.1029/2024JC021013, 2024.

https://doi.org/10.5194/egusphere-2026-4580
Preprint. Discussion started: 7 September 2026

Farrenkopf, A. M. and Luther, G. W.: Iodine chemistry reflects productivity and denitrification in the Arabian Sea: evidence for flux of dissolved species from sediments of western India into the OMZ, Deep Sea Research Part II: Topical Studies in Oceanography, 49, 2303-2318, https://doi.org/10.1016/S0967-0645(02)00038-3, 2002.

Farrenkopf, A. M., Dollhopf, M. E., Chadhain, S. N., Luther, G. W., and Nealson, K. H.: Reduction of iodate in seawater during Arabian Sea shipboard incubations and in laboratory cultures of the marine bacterium Shewanella putrefaciens strain MR-4, Mar. Chem., 57, 347-354, https://doi.org/10.1016/S0304-4203(97)00039-X, 1997.

Fuge, R. and Johnson, C. C.: Iodine and human health, the role of environmental geochemistry and diet, a review, Applied Geochemistry, 63, 282-302, https://doi.org/10.1016/j.apgeochem.2015.09.013, 2015.

Gantt, B., Sarwar, G., Xing, J., Simon, H., Schwede, D., Hutzell, W. T., Mathur, R., and Saiz-Lopez, A.: The Impact of Iodide-Mediated Ozone Deposition and Halogen Chemistry on Surface Ozone Concentrations Across the Continental United States, Environ. Sci. Technol., 51, 1458-1466, 10.1021/acs.est.6b03556, 2017.

Gómez Martín, J. C., Lewis, T. R., James, A. D., Saiz-Lopez, A., and Plane, J. M. C.: Insights into the Chemistry of Iodine New Particle Formation: The Role of Iodine Oxides and the Source of Iodic Acid, J. Am. Chem. Soc., 144, 9240-9253, 10.1021/jacs.1c12957, 2022.

Good, P., Sellar, A., Tang, Y., Rumbold, S., Ellis, R., Kelley, D., and Kuhlbrodt, T.: MOHC UKESM1.0-LL model output prepared for CMIP6 ScenarioMIP ssp585, Earth System Grid Federation [dataset], 10.22033/ESGF/CMIP6.6405, 2019.

Hardisty, D. S., Horner, T. J., Wankel, S. D., Blusztajn, J., and Nielsen, S. G.: Experimental observations of marine iodide oxidation using a novel sparge-interface MC-ICP-MS technique, Chem. Geol., 532, 119360, https://doi.org/10.1016/j.chemgeo.2019.119360, 2020.

Hardisty, D. S., Horner, T. J., Evans, N., Moriyasu, R., Babbin, A. R., Wankel, S. D., Moffett, J. W., and Nielsen, S. G.: Limited iodate reduction in shipboard seawater incubations from the Eastern Tropical North Pacific oxygen deficient zone, Earth and Planetary Science Letters, 554, 116676, https://doi.org/10.1016/j.epsl.2020.116676, 2021.

He, P., Hou, X., Aldahan, A., Possnert, G., and Yi, P.: Iodine isotopes species fingerprinting environmental conditions in surface water along the northeastern Atlantic Ocean, Sci. Rep., 3, 2685, 10.1038/srep02685, 2013.

Hepach, H., Hughes, C., Hogg, K., Collings, S., and Chance, R.: Senescence as the main driver of iodide release from a diverse range of marine phytoplankton, Biogeosciences, 17, 2453-2471, 10.5194/bg-17-2453-2020, 2020.

Huang, Z., Ito, K., Morita, I., Yokota, K., Fukushi, K., Timerbaev, A. R., Watanabe, S., and Hirokawa, T.: Sensitive monitoring of iodine species in sea water using capillary electrophoresis: vertical profiles of dissolved iodine in the Pacific Ocean, J. Environ. Monit., 7, 804-808, 10.1039/b501398d, 2005.

Hughes, C., Barton, E., Hepach, H., Chance, R., Pickering, M. D., Hogg, K., Pommerening-Röser, A., Wadley, M. R., Stevens, D. P., and Jickells, T. D.: Oxidation of iodide to iodate by cultures of marine ammonia-oxidising bacteria, Mar. Chem., 234, 104000, https://doi.org/10.1016/j.marchem.2021.104000, 2021.

Jia-Zhong, Z. and Whitfield, M.: Kinetics of inorganic redox reactions in seawater: I. The reduction of iodate by bisulphide, Mar. Chem., 19, 121-137, https://doi.org/10.1016/0304-4203(86)90044-7, 1986.

https://doi.org/10.5194/egusphere-2026-4580
Preprint. Discussion started: 7 September 2026

Jickells, T. D., Deuser, W. G., and Belastock, R. A.: Temporal variations in the concentrations of some particulate elements in the surface waters of the Sargasso Sea and their relationship to deep-sea fluxes, Mar. Chem., 29, 203-219, https://doi.org/10.1016/0304-4203(90)90014-4, 1990.

Jones, M. R., Chance, R., Bell, T., Jones, O., Loades, D. C., May, R., Tinel, L., Weddell, K., Widdicombe, C., and Carpenter, L. J.: Iodide, iodate & dissolved organic iodine in the temperate coastal ocean, Frontiers in Marine Science, 11, 10.3389/fmars.2024.1277595, 2024.

Kuhlbrodt, T., Jones, C. G., Sellar, A., Storkey, D., Blockley, E., Stringer, M., Hill, R., Graham, T., Ridley, J., Blaker, A., Calvert, D., Copsey, D., Ellis, R., Hewitt, H., Hyder, P., Ineson, S., Mulcahy, J., Siahaan, A., and Walton, J.: The Low-Resolution Version of HadGEM3 GC3.1: Development and Evaluation for Global Climate, Journal of Advances in Modeling Earth Systems, 10, 2865-2888, https://doi.org/10.1029/2018MS001370, 2018.

Küpper, F. C., Carpenter, L. J., McFiggans, G. B., Palmer, C. J., Waite, T. J., Boneberg, E.-M., Woitsch, S., Weiller, M., Abela, R., Grolimund, D., Potin, P., Butler, A., Luther, G. W., Kroneck, P. M. H., Meyer-Klaucke, W., and Feiters, M. C.: Iodide accumulation provides kelp with an inorganic antioxidant impacting atmospheric chemistry, Proceedings of the National Academy of Sciences, 105, 6954-6958, doi:10.1073/pnas.0709959105, 2008.

Kwiatkowski, L., Torres, O., Bopp, L., Aumont, O., Chamberlain, M., Christian, J. R., Dunne, J. P., Gehlen, M., Ilyina, T., John, J. G., Lenton, A., Li, H., Lovenduski, N. S., Orr, J. C., Palmieri, J., Santana-Falcón, Y., Schwinger, J., Séférian, R., Stock, C. A., Tagliabue, A., Takano, Y., Tjiputra, J., Toyama, K., Tsujino, H., Watanabe, M., Yamamoto, A., Yool, A., and Ziehn, T.: Twenty-first century ocean warming, acidification, deoxygenation, and upper-ocean nutrient and primary production decline from CMIP6 model projections, Biogeosciences, 17, 3439-3470, 10.5194/bg-17-3439-2020, 2020.

Lawrence, B. N., Bennett, V. L., Churchill, J., Juckes, M., Kershaw, P., Pascoe, S., Pepler, S., Pritchard, M., and Stephens, A.: Storing and manipulating environmental big data with JASMIN, 2013 IEEE International Conference on Big Data, 6-9 Oct. 2013, 68-75, 10.1109/BigData.2013.6691556,

Laws, E. A., Falkowski, P. G., Smith Jr, W. O., Ducklow, H., and McCarthy, J. J.: Temperature effects on export production in the open ocean, Global Biogeochemical Cycles, 14, 1231-1246, https://doi.org/10.1029/1999GB001229, 2000.

Lee, H., Moon, B.-K., Jung, H.-C., Park, J.-Y., Shim, S., La, N., Kim, A.-H., Yum, S. S., Ha, J.-C., Byun, Y.-H., Sung, H. M., and Lee, J.: Development of the UKESM-TOPAZ Earth System Model (Version 1.0) and Preliminary Evaluation of its Biogeochemical Simulations, Asia-Pacific Journal of Atmospheric Sciences, 58, 379-400, 10.1007/s13143-021-00263-0, 2022.

Legrand, M., McConnell, J. R., Preunkert, S., Arienzo, M., Chellman, N., Gleason, K., Sherwen, T., Evans, M. J., and Carpenter, L. J.: Alpine ice evidence of a three-fold increase in atmospheric iodine deposition since 1950 in Europe due to increasing oceanic emissions, Proceedings of the National Academy of Sciences, 115, 12136-12141, doi:10.1073/pnas.1809867115, 2018.

Longhurst, A. R.: Ecological Geography of the Sea,

https://doi.org/10.5194/egusphere-2026-4580
Preprint. Discussion started: 7 September 2026

Lu, W., Ridgwell, A., Thomas, E., Hardisty, D. S., Luo, G., Algeo, T. J., Saltzman, M. R., Gill, B. C., Shen, Y., Ling, H.-F., Edwards, C. T., Whalen, M. T., Zhou, X., Gutchess, K. M., Jin, L., Rickaby, R. E. M., Jenkyns, H. C., Lyons, T. W., Lenton, T. M., Kump, L. R., and Lu, Z.: Late inception of a resiliently oxygenated upper ocean, Science, 361, 174-177, doi:10.1126/science.aar5372, 2018.

Lu, Z., Hoogakker, B. A. A., Hillenbrand, C.-D., Zhou, X., Thomas, E., Gutchess, K. M., Lu, W., Jones, L., and Rickaby, R. E. M.: Oxygen depletion recorded in upper waters of the glacial Southern Ocean, Nature Communications, 7, 11146, 10.1038/ncomms11146, 2016.

Luther, G. W.: Review on the physical chemistry of iodine transformations in the oceans, Frontiers in Marine Science, 10, 10.3389/fmars.2023.1085618, 2023.

MacDonald, S. M., Gómez Martín, J. C., Chance, R., Warriner, S., Saiz-Lopez, A., Carpenter, L. J., and Plane, J. M. C.: A laboratory characterisation of inorganic iodine emissions from the sea surface: dependence on oceanic variables and parameterisation for global modelling, Atmos. Chem. Phys., 14, 5841-5852, 10.5194/acp-14-5841-2014, 2014.

Madec, G.: NEMO ocean engine [code], https://doi.org/10.5281/zenodo.1472492, 2017.

Marbà, N., Duarte, C. M., and Agustí, S.: Allometric scaling of plant life history, Proceedings of the National Academy of Sciences, 104, 15777-15780, 10.1073/pnas.0703476104, 2007.

Moisan, T. A., Dunstan, W. M., Udomkit, A., and Wong, G. T. F.: The uptake of iodate by marine phytoplankton, Journal of Phycology, 30, 580-587, https://doi.org/10.1111/j.0022-3646.1994.00580.x, 1994.

Moriyasu, R., Evans, N., Bolster, K. M., Hardisty, D. S., and Moffett, J. W.: The Distribution and Redox Speciation of Iodine in the Eastern Tropical North Pacific Ocean, Global Biogeochemical Cycles, 34, e2019GB006302, https://doi.org/10.1029/2019GB006302, 2020.

Moriyasu, R., Bolster, K. M., Hardisty, D. S., Kadko, D. C., Stephens, M. P., and Moffett, J. W.: Meridional Survey of the Central Pacific Reveals Iodide Accumulation in Equatorial Surface Waters and Benthic Sources in the Abyssal Plain, Global Biogeochemical Cycles, 37, e2021GB007300, https://doi.org/10.1029/2021GB007300, 2023.

O'Dowd, C. D., Jimenez, J. L., Bahreini, R., Flagan, R. C., Seinfeld, J. H., Hämeri, K., Pirjola, L., Kulmala, M., Jennings, S. G., and Hoffmann, T.: Marine aerosol formation from biogenic iodine emissions, Nature, 417, 632-636, 10.1038/nature00775, 2002.

Pound, R.: the new one, Science Advances, 2026.

Pound, R. J., Brown, L. V., Evans, M. J., and Carpenter, L. J.: An improved estimate of inorganic iodine emissions from the ocean using a coupled surface microlayer box model, Atmos. Chem. Phys., 24, 9899-9921, 10.5194/acp-24-9899-2024, 2024.

Prados-Roman, C., Cuevas, C. A., Fernandez, R. P., Kinnison, D. E., Lamarque, J. F., and Saiz-Lopez, A.: A negative feedback between anthropogenic ozone pollution and enhanced ocean emissions of iodine, Atmos. Chem. Phys., 15, 2215-2224, 10.5194/acp-15-2215-2015, 2015.

https://doi.org/10.5194/egusphere-2026-4580
Preprint. Discussion started: 7 September 2026

Prasanna Kumar, S., Muraleedharan, P. M., Prasad, T. G., Gauns, M., Ramaiah, N., de Souza, S. N., Sardesai, S., and Madhupratap, M.: Why is the Bay of Bengal less productive during summer monsoon compared to the Arabian Sea?, Geophys. Res. Lett., 29, 88-81-88-84, https://doi.org/10.1029/2002GL016013, 2002.

Price, N. B. and Calvert, S. E.: The geochemistry of iodine in oxidised and reduced recent marine sediments, Geochim. Cosmochim. Acta, 37, 2149-2158, https://doi.org/10.1016/0016-7037(73)90013-6, 1973.

Rapp, I., Schlosser, C., Browning, T. J., Wolf, F., Le Moigne, F. A. C., Gledhill, M., and Achterberg, E. P.: El Niño-Driven Oxygenation Impacts Peruvian Shelf Iron Supply to the South Pacific Ocean, Geophys. Res. Lett., 47, e2019GL086631, https://doi.org/10.1029/2019GL086631, 2020.

Rapp, I., Schlosser, C., Menzel Barraqueta, J. L., Wenzel, B., Lüdke, J., Scholten, J., Gasser, B., Reichert, P., Gledhill, M., Dengler, M., and Achterberg, E. P.: Controls on redox-sensitive trace metals in the Mauritanian oxygen minimum zone, Biogeosciences, 16, 4157-4182, 10.5194/bg-16-4157-2019, 2019.

Reyes-Umana, V., Henning, Z., Lee, K., Barnum, T. P., and Coates, J. D.: Genetic and phylogenetic analysis of dissimilatory iodate-reducing bacteria identifies potential niches across the world's oceans, The ISME Journal, 16, 38-49, 10.1038/s41396-021-01034-5, 2022.

Rue, E. L., Smith, G. J., Cutter, G. A., and Bruland, K. W.: The response of trace element redox couples to suboxic conditions in the water column, Deep Sea Research Part I: Oceanographic Research Papers, 44, 113-134, https://doi.org/10.1016/S0967-0637(96)00088-X, 1997.

Satoh, Y., Otosaka, S., Suzuki, T., and Nakanishi, T.: Factors regulating the concentration of particulate iodine in coastal seawater, Limnology and Oceanography, 68, 1580-1594, https://doi.org/10.1002/lno.12369, 2023.

Schmidtko, S., Stramma, L., and Visbeck, M.: Decline in global oceanic oxygen content during the past five decades, Nature, 542, 335-339, 10.1038/nature21399, 2017.

Schnur, A. A., Sutherland, K. M., Hansel, C. M., and Hardisty, D. S.: Rates and pathways of iodine speciation transformations at the Bermuda Atlantic Time Series, Frontiers in Marine Science, 10, 10.3389/fmars.2023.1272870, 2024.

Sellar, A. A., Jones, C. G., Mulcahy, J. P., Tang, Y., Yool, A., Wiltshire, A., O'Connor, F. M., Stringer, M., Hill, R., Palmieri, J., Woodward, S., de Mora, L., Kuhlbrodt, T., Rumbold, S. T., Kelley, D. I., Ellis, R., Johnson, C. E., Walton, J., Abraham, N. L., Andrews, M. B., Andrews, T., Archibald, A. T., Berthou, S., Burke, E., Blockley, E., Carslaw, K., Dalvi, M., Edwards, J., Folberth, G. A., Gedney, N., Griffiths, P. T., Harper, A. B., Hendry, M. A., Hewitt, A. J., Johnson, B., Jones, A., Jones, C. D., Keeble, J., Liddicoat, S., Morgenstern, O., Parker, R. J., Predoi, V., Robertson, E., Siahaan, A., Smith, R. S., Swaminathan, R., Woodhouse, M. T., Zeng, G., and Zerroukat, M.: UKESM1: Description and Evaluation of the U.K. Earth System Model, Journal of Advances in Modeling Earth Systems, 11, 4513-4558, https://doi.org/10.1029/2019MS001739, 2019.

Shaikh, A., Kurian, S., Shenoy, D. M., Pratihary, A. K., and Shetye, S. S.: Biogeochemical cycling of iodine in the Bay of Bengal: A comparison with the Arabian Sea, Mar. Pollut. Bull., 209, 117329, https://doi.org/10.1016/j.marpolbul.2024.117329, 2024.

https://doi.org/10.5194/egusphere-2026-4580
Preprint. Discussion started: 7 September 2026

Shaikh, A., Kurian, S., Shenoy, D. M., Pratihary, A. K., Dais, A. B., Naik, R., and Borker, S. G.: Spatial and temporal variation of dissolved iodine in the eastern Arabian Sea, Mar. Chem., 257, 104322, https://doi.org/10.1016/j.marchem.2023.104322, 2023.

Sherwen, T., Chance, R. J., Tinel, L., Ellis, D., Evans, M. J., and Carpenter, L. J.: A machine-learning-based global sea-surface iodide distribution, Earth Syst. Sci. Data, 11, 1239-1262, 10.5194/essd-11-1239-2019, 2019.

Stramma, L., Johnson, G. C., Sprintall, J., and Mohrholz, V.: Expanding Oxygen-Minimum Zones in the Tropical Oceans, Science, 320, 655-658, 10.1126/science.1153847, 2008.

Ştreangă, I.-M., Repeta, D. J., Blusztajn, J. S., and Horner, T. J.: Speciation and cycling of iodine in the subtropical North Pacific Ocean, Frontiers in Marine Science, 10, 10.3389/fmars.2023.1272968, 2024.

Tang, W., Ward, B. B., Beman, M., Bristow, L., Clark, D., Fawcett, S., Frey, C., Fripiat, F., Herndl, G. J., Mdutyana, M., Paulot, F., Peng, X., Santoro, A. E., Shiozaki, T., Sintes, E., Stock, C., Sun, X., Wan, X. S., Xu, M. N., and Zhang, Y.: Database of nitrification and nitrifiers in the global ocean, Earth Syst. Sci. Data, 15, 5039-5077, 10.5194/essd-15-5039-2023, 2023.

Tang, Y., Rumbold, S., Ellis, R., Kelley, D., Mulcahy, J., Sellar, A., Walton, J., and Jones, C.: MOHC UKESM1.0-LL model output prepared for CMIP6 CMIP piControl, Earth System Grid Federation [dataset], 10.22033/ESGF/CMIP6.6298, 2019.

Truesdale, V. W.: A re-assessment of redfield correlations between dissolved iodine and nutrients in oceanic waters and a strategy for further investigations of iodine, Mar. Chem., 48, 43-56, https://doi.org/10.1016/0304-4203(94)90061-2, 1994.

Truesdale, V. W., Watts, S. F., and Rendell, A. R.: On the possibility of iodide oxidation in the near-surface of the Black Sea and its implications to iodine in the general ocean, Deep Sea Research Part I: Oceanographic Research Papers, 48, 2397-2412, https://doi.org/10.1016/S0967-0637(01)00021-8, 2001.

Tsunogai, S.: Iodine in the deep water of the ocean, Deep Sea Research and Oceanographic Abstracts, 18, 913-919, https://doi.org/10.1016/0011-7471(71)90065-9, 1971.

Ullman, W. J. and Aller, R. C.: The geochemistry of iodine in near-shore carbonate sediments, Geochim. Cosmochim. Acta, 49, 967-978, https://doi.org/10.1016/0016-7037(85)90311-4, 1985.

van Bergeijk, S. A., Hernández, L., Zubía, E., and Cañavate, J. P.: Iodine balance, growth and biochemical composition of three marine microalgae cultured under various inorganic iodine concentrations, Mar. Biol., 163, 107, 10.1007/s00227-016-2884-0, 2016.

Wadley M.R., Chance R., Pound R.J. and Stevens D.P.: Global ocean iodide and iodate concentration for present day (2000-2019), historical (1880-1899) and future (2080-2099 under SSP585 scenario) generated using the I-CYCLE global ocean model of iodine cycling. NERC EDS British Oceanographic Data Centre NOC. doi:10.5285/561a6d79-2192-7b77-e063-7086abc0ecb5, 2026.

Wadley, M. R., Stevens, D. P., Jickells, T. D., Hughes, C., Chance, R., Hepach, H., Tinel, L., and Carpenter, L. J.: A Global Model for Iodine Speciation in the Upper Ocean, Global Biogeochemical Cycles, 34, e2019GB006467, https://doi.org/10.1029/2019GB006467, 2020.

https://doi.org/10.5194/egusphere-2026-4580
Preprint. Discussion started: 7 September 2026

Webb, A. L., Oudova-Rivera, B., Ward, M., Carpenter, L. J., Lehtovirta-Morley, L. E., and Chance, R.: The Ammonia Oxidising Archaeon Nitrosopumilus maritimus Does Not Alter Iodine Oxidation State in Oxic Seawater, Environ. Microbiol. Rep., 17, e70168, https://doi.org/10.1111/1758-2229.70168, 2025.

Winkelbauer, H. A., Hoogakker, B. A. A., Chance, R. J., Davis, C. V., Anthony, C. J., Bischoff, J., Carpenter, L. J., Chenery, S. R. N., Hamilton, E. M., Holdship, P., Peck, V. L., Poulton, A. J., Stinchcombe, M. C., and Wishner, K. F.: Planktic foraminifera iodine/calcium ratios from plankton tows, Frontiers in Marine Science, 10, 10.3389/fmars.2023.1095570, 2023.

Wong, G. T. F.: The marine geochemistry of iodine, Reviews in Aquatic Sciences, 4, 45-73, 1991.

Wong, G. T. F.: Coupling iodine speciation to primary, regenerated or "new" production: a re-evaluation, Deep Sea Research Part I: Oceanographic Research Papers, 48, 1459-1476, https://doi.org/10.1016/S0967-0637(00)00097-2, 2001.

Wong, G. T. F. and Brewer, P. G.: The marine chemistry of iodine in anoxic basins, Geochim. Cosmochim. Acta, 41, 151-159, https://doi.org/10.1016/0016-7037(77)90195-8, 1977.

Wong, G. T. F. and Cheng, X.-H.: Dissolved organic iodine in marine waters: Determination, occurrence and analytical implications, Mar. Chem., 59, 271-281, https://doi.org/10.1016/S0304-4203(97)00078-9, 1998.

Wong, G. T. F. and Hung, C.-C.: Speciation of dissolved iodine: integrating nitrate uptake over time in the oceans, Continental Shelf Research, 21, 113-128, https://doi.org/10.1016/S0278-4343(00)00086-8, 2001.

Wong, G. T. F. and Zhang, L.-S.: Seasonal variations in the speciation of dissolved iodine in the Chesapeake Bay, Estuarine, Coastal and Shelf Science, 56, 1093-1106, https://doi.org/10.1016/S0272-7714(02)00310-4, 2003.

Wong, G. T. F., Brewer, P. G., and Spencer, D. W.: The distribution of particulate iodine in the Atlantic Ocean, Earth and Planetary Science Letters, 32, 441-450, https://doi.org/10.1016/0012-821X(76)90084-4, 1976.

Yool, A., Popova, E. E., and Anderson, T. R.: MEDUSA-2.0: an intermediate complexity biogeochemical model of the marine carbon cycle for climate change and ocean acidification studies, Geosci. Model Dev., 6, 1767-1811, 10.5194/gmd-6-1767-2013, 2013.

Yool, A., Martin, A. P., Fernández, C., and Clark, D. R.: The significance of nitrification for oceanic new production, Nature, 447, 999-1002, 10.1038/nature05885, 2007.

Zhang, L., Hou, X., Gwynn, J. P., Karcher, M., Chen, N., Fan, Y., and Liu, Q.: Spatial variation and species transformation of 129I and 127I in the Central Arctic Ocean, Earth and Planetary Science Letters, 612, 118165, https://doi.org/10.1016/j.epsl.2023.118165, 2023.

Žic, V., Carić, M., and Ciglenečki, I.: The impact of natural water column mixing on iodine and nutrient speciation in a eutrophic anchialine pond (Rogoznica Lake, Croatia), Estuarine, Coastal and Shelf Science, 133, 260-272, https://doi.org/10.1016/j.ecss.2013.09.008, 2013.

Zimmermann, M. B., Jooste, P. L., and Pandav, C. S.: Iodine-deficiency disorders, The Lancet, 372, 1251-1262, https://doi.org/10.1016/S0140-6736(08)61005-3, 2008.